# A Process and Investigation into the Influence of Cast Surface Condition on Fatigue Life

by

**Jeffrey Tscherter**

A thesis submitted to the graduate faculty

in partial fulfillment of the requirements for the degree of

MASTER OF SCIENCE

Major: Industrial Engineering

Program of Study Committee:
Frank Peters, Major Professor
Matthew Frank
David Eisenmann

The student author, whose presentation of the scholarship herein was approved by the program of study committee, is solely responsible for the content of this thesis. The Graduate College will ensure this thesis is globally accessible and will not permit alterations after a degree is conferred.

Iowa State University

Ames, Iowa

2020

## DEDICATION

I dedicate this thesis to my parents and wife, who have all provided unwavering support throughout my undergraduate and graduate coursework. Without them, I would not be in the position I am today.

## TABLE OF CONTENTS

## LIST OF TABLES

## LIST OF FIGURES

# ACKNOWLEDGMENTS

I would like to thank my major professor, Dr. Frank Peters, for his mentorship throughout my academic career at Iowa State University. I would also like to thank my committee members, Dr. David Eisenmann and Dr. Matthew Frank for their guidance through this research. I want to thank Aaron Jordan and Doug Wood for their support and insight throughout the development of this study. Next, I want to acknowledge my lab mates: Ali Khorasani, Daniel Schimpf, Mitchell Nelsen, Eric Weflen, and Sharon Lau for their advice and support.

I want to thank the Steel Founders' Society of America for their support and funding. The advice received from them and Dr. Darrell Socie (University of Illinois), shaped this research. Also, I would like to thank Dr. Robin Foley and The University of Alabama at Birmingham for their contributions to this research. Finally, I would like to thank Hayley Brown from the Steel Founders' Society of America for her help in developing the final product of this research.

## ABSTRACT

The objective of this research is to investigate the impact of varying cast surface conditions on fatigue performance, in the presence of other casting indications such as gas and shrinkage porosity. Additionally, this research aims to draw connections between nondestructive evaluation (NDE) techniques and fatigue results of cast test specimens. A process of specimen manufacturing, processing, and inspection is presented in this research, along with fatigue testing results.

It is known that poor surface condition can impact fatigue life, even when comparing surface finishes produced by different manufacturing processes. Cast surface roughness is thought to contribute to reduced fatigue life, which may lead to over-processed or over-designed parts. Little has been done to investigate the impact of different cast surface conditions on fatigue life to justify current industry practices. Fatigue specimen design, inspection techniques, and fatigue testing techniques were developed in this study to compare the impact of cast surface condition on fatigue in the presence of other indications. To investigate this impact, axial load-controlled high-cycle fatigue tests were conducted on large lab-scale specimens cut from cast plates. All specimens underwent radiographic inspection, wet magnetic particle inspection, laser scanning, and visual surface characterization. Cast surfaces were characterized utilizing ASTM A802 comparator plates and through digital methods. Fatigue results showed no difference in mean fatigue lives produced by different surface classifications. Additionally, no correlation was found between digital surface classification and fatigue life. These results indicate that cast surface texture is a not reliable indicator of fatigue life. Post-test measurements of fatigue crack initiation sites provided statistically significant results in a log-log regression with fatigue life.

This shows that variation in fatigue performance for a given cast material can be explained by the size of casting indications.

# CHAPTER 1. INTRODUCTION AND LITERATURE REVIEW

Casting is one method used to produce steel parts. Cast steel parts are utilized in a variety of applications and industries demanding specific physical and mechanical properties. Fatigue life is one commonly considered property in the design of steel parts and can be vital in determining part performance. Surface condition is known to have some impact on fatigue through notches, discontinuities, or other stress concentrations. The extent of impact a cast surface finish has on parts when compared with internal porosity, surface porosity, or other indications is not well known. It is important to understand what is most likely to impact fatigue, so that extra time and money are not spent removing indications or smoothing a surface when other factors may have a larger impact.

The goals of this research are the following:

1. Develop a process to explore the impact of cast surfaces with common industry classifications on fatigue life
2. Compare the influence of surface condition with porosity and other indications on fatigue life
3. Utilize nondestructive evaluation (NDE) techniques to inspect test specimens and relate results to fatigue results

This thesis is divided into five chapters. The first provides an introduction to fatigue and nondestructive evaluation techniques with an emphasis on castings and surface finish. Chapter 2 covers the methods developed and conducted to address the research motivations mentioned above. Three covers results and four is a discussion of results, and five provides a summary of the results along with shortcomings, contributions, and future work.

## Fatigue

Fatigue failures are a primary failure mode in functional parts due to cyclic loading and unloading. Engineered components that are exposed to a load over time will undergo some fatigue. This is typically the reason for failure if the applied load was lower than the yield strength of the material, which is the stress at which plastic deformation occurs in a material. There are many determining factors in the fatigue performance of cast parts. Environmental factors including the magnitude and direction of an applied load, frequency of an applied load, corrosion and erosion, and temperature all impact fatigue performance. Physical factors are also known to impact fatigue performance such as material composition, micro- and macro-porosity, grain structure, hardness, and surface condition.

Fatigue failure occurs in three stages: initiation, stable crack propagation, and unstable crack propagation to failure. Total fatigue life is the sum of time spent in all three stages, starting from when a crack is visible. Due to defects inherent to manufacturing processes and materials, it is accepted that there are already crack-like features present in parts [1].

## Predicting Fatigue Life

Various fatigue laws, relationships, and methods are utilized to model and predict fatigue life. Stress-life, strain-life, and crack growth are all well-known approaches that are used to estimate fatigue performance. Stress-life is applicable during high cycle fatigue testing when the applied stress amplitude is within the elastic range of a material. Stress-Life (S-N) curves are a common method of plotting and predicting fatigue lives for a given material (Figure 1 [2]). These curves are produced through destructive testing for a specific material and stress amplitude. Developed curves may not be an accurate representation of loading conditions in industry, since tests are performed under controlled conditions [3].

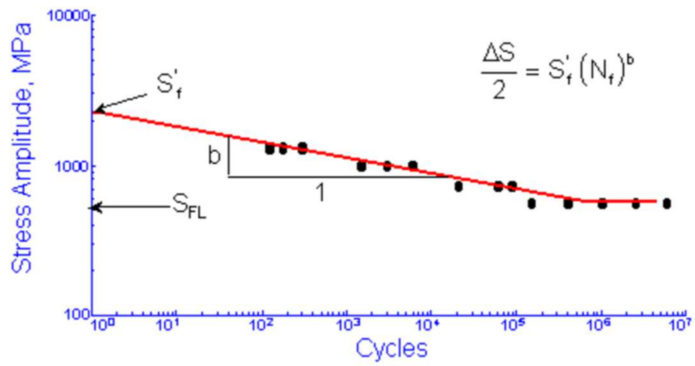


Figure 1: S-N curve showing cyclic stress on the y-axis and number of cycles to failure on the x-axis

Basquin's equation is used to describe fatigue life in ($N_f$) by the applied alternating stress $S_a$ on a log-log stress-life plot (S-N curve). This relationship can be used to describe fatigue life up to the fatigue limit of a material, which is the stress a material can experience for an infinite number of cycles. This relationship between alternating stress and fatigue life is shown below in Equation 1 where $A$ and $B$ are material constants.

$$S_a = A\left(N_f\right)^B \tag{1}$$

Strain-life is an approach used to describe fatigue life where plastic deformation is a factor in performance and considers the stress-strain relationship of cyclic loading. The Manson-Coffin relationship, which is shown in Equation 2 relates the plastic strain amplitude ($\frac{\Delta\varepsilon_p}{2}$) to the cycles of failure ($N_f$) on a log-log strain-life plot. In this equation, $\varepsilon'_f$ is the fatigue ductility coefficient and $c$ is the fatigue ductility exponent, which are both material properties. This relationship is found to hold for many ductile metallic materials, although some exhibit a bilinear relationship and possess a linearity transition point [4].

$$\frac{\Delta \varepsilon_p}{2} = \varepsilon'_f \left(N_f\right)^c \tag{2}$$

Elastic and plastic strains can be applied to the relationship between reversals to failure ($N_f$) and strain amplitude ($\frac{\Delta\varepsilon}{2}$) for total fatigue life shown in Equation 3 [5]. In this equation, $\sigma'_f$ is the fatigue strength coefficient, E is the elastic modulus, $\varepsilon'_f$ is the fatigue ductility coefficient, $c$ is the fatigue ductility exponent, and $b$ is the fatigue strength exponent.

$$\frac{\Delta \varepsilon}{2} = \frac{\sigma'_f}{E}\left(2N_f\right)^b + \varepsilon'_f\left(2N_f\right)^c \tag{3}$$

Fatigue life can also be estimated by crack growth rate ($\frac{da}{dN}$). The Paris law relates the crack growth rate to stress intensity factor ($\Delta K$) as shown in Equation 4 [6]. This relationship is also plotted in Figure 2 [7]. *C* and *m* are experimentally determined constants. Integrating this equation with respect to *da* and substituting $\Delta K$ provides an equation relating the number of cycles to get from a crack of initial size $a_0$ to final crack size $a_f$ shown in Equation 5. In this equation, $\Delta S$ is the stress amplitude and *Y* is a geometry factor (which is assumed to be constant for integration).

$$\frac{da}{dN} = C\Delta K^m \tag{4}$$

$$N_{a_0 \to a_f} = \frac{2}{(m-2)C(\Delta SY)^m \pi^{\frac{m}{2}}}\left[\frac{1}{a_0^{\frac{m-2}{2}}} - \frac{1}{a_f^{\frac{m-2}{2}}}\right] \tag{5}$$

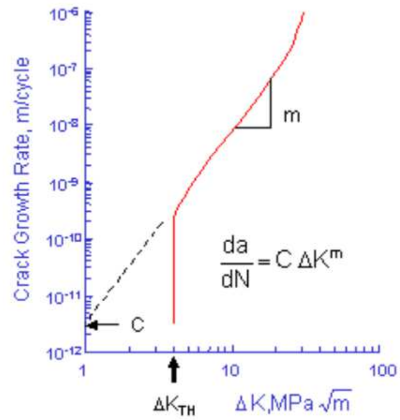


Figure 2: Crack growth rate by stress intensity

New models and methods are continuously being developed to predict fatigue life. In a review of fatigue life prediction methods by Satnecchia et al., prediction models fall into the following categories: linear damage rule-based, multiaxial and variable amplitude loading, stochastic-based, energy-based, and continuum damage mechanics [8]. To consider the impact of surface condition, a few examples of these models use the density of surface and non-surface inclusions as a statistical parameter in a probabilistic approach to estimate fatigue life [9] [10] [11] [12]. Horikawa et al. used surface roughness measurements to estimate the fatigue lives of thin-wall cast-iron specimens with some success [13]. Their use of thin-walled cast specimens, however, does not apply as well to fatigue life prediction methods for large cast parts since fracture toughness changes with material thickness and hardness [14]. Kyrre Ås et al. utilized finite element analysis (FEA) to analyze surface roughness and subsurface stress fields. These analyses were used to successfully identify critical locations for fatigue crack initiation in notched aluminum specimens. The use of subsurface stress fields proved as the most capable method of identifying critical locations [15]. Within this research, the crack-growth Paris law approach was utilized to analyze fatigue failures. This method provides the simplest and most applicable means to evaluate fatigue failures produced through the testing methods used in this study.

Despite multiple methods being available to predict fatigue life, it is still difficult to determine part performance from inspection techniques. As stated by Blair et al., safety factors are often used to ensure cast parts meet performance requirements. Variability in the casting process and current capabilities of NDE techniques make it difficult to develop prediction models to accurately predict fatigue lives of cast parts [16]. This research aims to explain how surface, near-surface, and internal condition of steel castings relate to fatigue performance. Additionally, links between those results and NDE results are explored in this study, to improve fatigue life prediction techniques based on inspections of cast parts.

## Nondestructive Evaluation (NDE) of Castings

Nondestructive evaluation or nondestructive testing (NDT) is utilized to inspect the quality of castings. Example NDE techniques are visual inspection, digital inspection (laser scanning), magnetic particle inspection (MPI), radiography, and ultrasound. NDE techniques have varying abilities in terms of what indications they can detect in a casting and how effectively they can classify those indications. Consequently, the ability to predict casting performance varies between each technique. As explained in "Predicting the Occurrence and Effects of Defects in Castings" by Blair et al., qualitative factors from inspection results lead to conservative design rules [16]. These conservative design rules are intended to provide some factor of safety in the design of a steel casting. Excessive safety factors applied throughout the design and casting process can result in overdesigned products, leading to parts that may be heavier, more expensive, or take longer to manufacture. In a study by Choi et al., twelve castings from different commercial applications were tested and failed at loads four to twenty times the maximum service load [17]. Overperforming castings present an opportunity for cost and weight reduction. Through this research, NDE is identified as a possible method to address overprocessed and overperforming castings. Linking NDE results with fatigue can give inspectors a better ability to infer part performance through inspection and allow for parts to be designed without excessive safety factors.

Visual inspection is the most common NDE method in the casting process. Visual inspection is critical to the casting process due to the number of times it is conducted and its potential impact on processing time and cost. In casting, visual inspection is used to identify indications like non-metallic inclusions, surface irregularities, and to evaluate surface condition. Visual aids, like comparator plates, set the standard by which castings are evaluated for surface quality. As identified by Daricilar et al., there is no consistent and reliable method to communicate surface quality requirements through all steps of casting purchasing and production. This leads to the possibility of overprocessing or missed defects. Daricilar also quantified the repeatability and reproducibility errors in visual inspections of steel casting surfaces [18]. This variability can be partially attributed to environmental, individual, and task factors inherent to inspection in the casting industry [19]. Connections between visually inspected casting attributes and casting performance are difficult to make considering the variability of the visual inspection process. Furthermore, the lack of research into the impact of varying cast surfaces on the mechanical properties of a part provides no basis for an inspector to infer how the part will perform based on visual inspection alone.

Digital methods such as laser scanning and surface evaluation algorithms provide an opportunity to reduce the amount of variability in surface inspection. In turn, these methods provide a standardized and quantitative approach to evaluate cast surfaces and relate them to mechanical properties. Voelker and Peters identified the need for a quantitative standard to evaluate cast surfaces, indicating current qualitative methods as too variable for effective communication [20]. Voelker proposed a standard that was intended to provide objective means for a customer to effectively communicate cast surface specifications to a manufacturer. In this approach, three different parameters are utilized to characterize a surface. These parameters are baseline roughness, abnormality level, and abnormality percentage. Baseline roughness is the typical $S_a$ (areal) or $R_a$ (profile) in mm associated with a surface. Abnormality level covers any surface feature that exceeds twice the baseline roughness measurement. This parameter is specified in mm and represents deviation from the underlying geometry. The abnormality percentage represents the ratio of abnormal to normal surface area as specified by the abnormality level [21]. An all-encompassing surface characterization standard like this could provide a better base by which to link estimated mechanical properties with cast surface characterization. Building on the work of Voelker, Schimpf and Peters developed the Variogram roughness method to evaluate casting surfaces. This method uses x, y, and z points and associated spatial information to determine a roughness value for a surface; with improvements in repeatability and reproducibility over visual inspection and an improved ability to differentiate surfaces over already developed surface standards [22]. Within this research, the Variogram roughness method is utilized as a new quantitative method to classify surface roughness and to draw a connection to fatigue life.

Magnetic particle inspection is another common NDE technique used to evaluate the surface and near-surface condition of ferromagnetic materials. MPI utilizes magnetic fields and magnetic particles on a part to identify surface and near-surface indications such as cracks and porosity via magnetic flux leakage [23]. These surface and sub-surface indications identifiable by MPI can negatively affect fatigue life by serving as stress concentrations and fatigue crack initiation sites. A study by Zheng et al. investigated the use of MPI and ultrasonic inspection (which is out of the scope of this research) for time-dependent reliability analysis of structures. They concluded that there is significant uncertainty related to the NDE techniques that have a strong influence on reliability analysis and suggest that decisions made using NDE results should also consider probabilistic information of the NDE method. Probabilistic information associated with the NDE techniques, in this study, are probability of detection and indication sizing error [24]. Information like this should be considered when trying to evaluate indications that may influence fatigue life.

Radiography is utilized to inspect internal features of castings. Internal porosity or other indications are the intended targets of radiography, and all can impact fatigue life as explained in the next section. Like other NDE methods, casting evaluation through radiography is a subjective process relying on visual comparisons of part and reference radiographs [25]. This makes it difficult to relate a quantitative result with a physical property of a casting such as estimated fatigue performance. Blair et al. have proposed a new quantitative standard to use as a method of characterizing indications on radiographs [25]. Standards like this may allow for an improved connection between internal indications and projected fatigue properties.

## Impacts of Porosity and Microstructure on Fatigue Life

Porosity due to shrinkage, gas, etc. is a physical property of castings that can have an impact on fatigue life. In bending fatigue, non-centerline shrinkage porosity was found to decrease the fatigue properties of cast steel sections, especially when the shrinkage porosity extended to the surface. Shrinkage also decreased the torsion fatigue strength of cast specimens [26]. Sigl et al. conducted axial fatigue tests on specimens containing varying levels of porosity. Fatigue limits were found to be much lower than sound cast material. Microporosity also caused a decrease in ductility, which led to much larger observed elastic strain amplitudes than plastic strain amplitudes. This caused brittle behavior and quicker crack growth rates. As a result, lower fatigue strength was observed at all strain amplitudes for microporosity specimens. This impact was also modeled by treating porosity as spherical notches and agreed with the test data [27]. The potential impact of near-surface porosity was evaluated in a finite-element modeling study conducted by Borbély et al. They found that large a large stress concentration can be developed due to a small amount of material between a free surface and near-surface indication if they are close enough. This may cause a fatigue crack to initiate at the sub-surface cavity [28].

Material grain structure also impacts fatigue life and fatigue crack propagation. Grain boundaries can act as barriers to fatigue crack propagation but can also serve as stress concentrators. In torsion and bending fatigue tests of 100CrMnMoSi6 steel, bainitic and martensitic microstructures were evaluated in low cycle fatigue (less than $10^5$ cycles) and high cycle fatigue. A bainitic structure displayed higher fatigue strength than martensitic specimens for low cycle fatigue with no difference in high cycle fatigue failures. This is most likely due to the brittleness of the martensitic specimens. In this study, it was concluded that the harder steels are more sensitive to surface crack initiation [29].

## Effect of Surface Finish on Fatigue

Surface finish is known to influence fatigue life, as indicated in multiple studies. In the *Atlas of Fatigue Curves*, it is stated that all fatigue cracks will initiate at the surface unless case hardening or internal defects are present [30]. In a study by Lipson and Noll, the impact of varying surface conditions (ground, machined, hot rolled, and as forged) on fatigue performance was evaluated. They found that with improved surface condition, fatigue limit increased when plotted against ultimate tensile strength [31]. A study by Evans and Ebert found that polished and lathe-turned surfaces improve the endurance limit in cast specimens when compared to an as-cast surface finish [32]. In addition to testing surface finish, centerline shrinkage was identified as a non-influential factor on bending fatigue life. This study did not indicate what the surface roughness was of the as-cast specimens, nor the methods by which they were cast. An R.R Moore Rotating Beam Testing Machine was used in these fatigue tests. Through this testing method, bending stresses are induced into the test specimen, magnifying any stress concentrators on the surface and masking any internal indications like centerline shrinkage. This testing method is the reason why centerline shrinkage did not affect fatigue life, according to the study. Additionally, specimens were cast out-of-round, leading to inertial stresses that may have caused premature failure. Considering this, Evans and Ebert stated that the extent of influence of an as-cast surface finish has on decreased fatigue life could not be determined.

A similar study was conducted on nodular cast iron by Koneþná et al. They also determined that an as-cast surface reduced bending fatigue life when compared to a fine-ground specimen. These findings were attributed to a difference in microstructure between cast surface and base metal layers. Fine-ground specimen lifetimes were dominated by fatigue crack initiation, while shot blast and as-cast specimen lives were dominated by fatigue crack propagation [33]. This study does not go any further to characterize the primary causes of fatigue failure.

Horikawa et al. conducted fatigue tests on thin wall cast iron specimens and concluded that higher casting surface roughness negatively affects fatigue life [13]. Specimens in this study were thin walled (3mm thick) cast iron to compare cast surfaces to non-cast surfaces only. Due to the experimental design, the extent of impact a cast surface has in relation to other possible fatigue crack nucleation sites is still unknown in this study. Additionally, as stated previously, fracture toughness changes with material thickness making it difficult to generalize part performance from thin specimens [14].

In *Fundamentals of Metal Fatigue Analysis* by Bannantine et al., it is noted that surface finish will have a larger impact on finer-grained materials than coarse-grained materials. It is also noted that the surface finish will have less of an impact at shorter fatigue lives when crack propagation is the primary component of fatigue life. Surface irregularities also influence fatigue life serving as stress concentrators that eventually become crack nucleation sites [34].

Notched surfaces are also known to negatively impact fatigue life and can be summarized quantitatively through the notch sensitivity factory (q). $K_f$ is the fatigue strength reduction factor, which describes the effective stress concentration of a small notch. $K_t$ is the stress concentration factor which describes the magnitude of stress increase due to a stress concentration or notch. Besides material, $(q)$ varies based on notch size and shape, part size and shape, and loading characteristics so it cannot be thought of as a material constant [35]. Methods to determine the sensitivity of fatigue life to varying casting surface finishes, unlike notch sensitivity, have not been explored or developed to the author's knowledge beyond the sources evaluated above.

$$q = \frac{K_f - 1}{K_t - 1} \tag{6}$$

It is emphasized by Murakami that stress concentration due to cracks is different from stress concentration due to holes or notches. Since cracks have a sharp tip, the stress concentration becomes unbounded. This makes it unreasonable to estimate the stress concentration of a crack by the stress concentration at the tip [36]. Due to this, the stress intensity factor in the case of a crack describes the intensity of a stress field in the vicinity of the crack tip [36] [37]. In this case, the stress intensity factor $(K_I)$ can be related to the uniaxial tensile stress $(\sigma_0)$ and crack length ($a_0$, or half of a symmetrical crack of length $2a_0$) as shown in Equation 7. According to Murakami and Endo, a reasonable estimate for three-dimensional cracks or defects is $\sqrt{area}$ where the area is projected from an indication in the direction of maximum tensile stress [38]. Substituting into Equation 7 yields Equation 8.

$$K_I = \sigma_0\sqrt{\pi a} \tag{7}$$

$$K_I = \sigma_0\sqrt{\pi\sqrt{area}} \tag{8}$$

Many designers of castings have operated with the understanding that poor surface finish will result in poor part performance. While this is known when comparing machined, forged, and cast materials [32], the impact of surface finishes produced by different manufacturing techniques continues to be investigated. McKelvey and Fatemi found that surface finish factors for forged parts based on historical data resulted in overly conservative (shorter) fatigue life predictions when compared to experimental data [39]. The influence of surface finishes produced by different cutting techniques were evaluated by Diekhoff et al. They found that waterjet surfaces produce higher fatigue strength when compared to oxygen, plasma, and laser-cut specimens [40]. In a study conducted by Itoga et al., higher surface roughness of machined specimens negatively impacted fatigue life and fatigue limit. Additionally, the transition stress where crack initiation occurred internally instead of on the surface decreased with increased surface roughness [41]. For steel castings, little work has been done to investigate the impact of varying surface condition on fatigue life. This research aims to address current industry practices by investigating the effects of cast surface finish along with other casting properties on fatigue life.

# CHAPTER 2. METHODOLOGY

This section discusses the methods used throughout specimen manufacturing, inspection, and testing.

## Test Specimen Material and Casting

Cast and normalized WCB steel alloy was used in testing, which is the cast equivalent to 1020 steel. This alloy's chemical composition is shown in Table 1, and its physical properties are shown in Table 2.

Table 1: WCB Chemical Composition

| C | Mn | Si | Ni | Cr | Mo | Al | S | P | Cu | V |
|---|---|---|---|---|---|---|---|---|---|---|
| 0.23% | 0.87% | 0.52% | 0.08% | 0.11% | 0.03% | 0.04% | 0.004% | 0.011% | 0.07% | 0.01% |

Table 2: WCB Physical Properties Tested by Eagle Alloy

| Brinell Hardness | Ultimate Tensile Strength (PSI) | Yield Strength (PSI) | %Elongation | Reduction in Area (RIA) | Young's Modulus (kips/in$^2$) |
|---|---|---|---|---|---|
| 158 | 77,922 | 50,929 | 28% | 48% | 278 |

Steel plates were cast by Eagle Alloy (Figure 3 and Figure 4) and designed to have varying surface finishes, shrinkage porosity, and surface gas porosity. To avoid shrinkage porosity, plates were cast with a two-degree taper from the outside to the middle on both cope and drag sides.

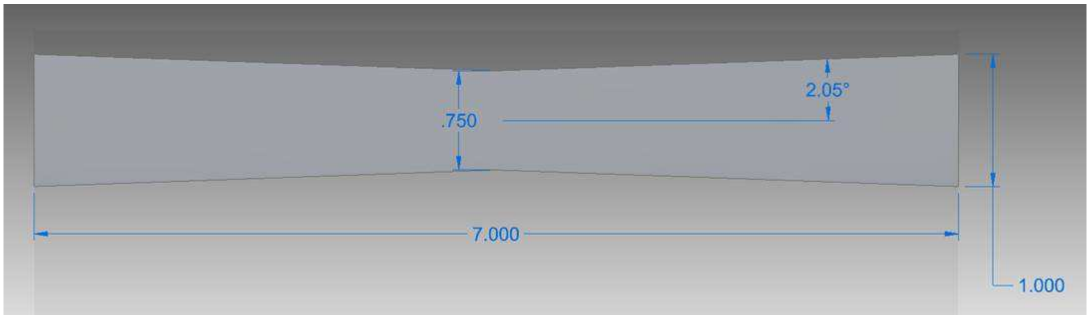


Figure 3: Cast plate profile dimensions

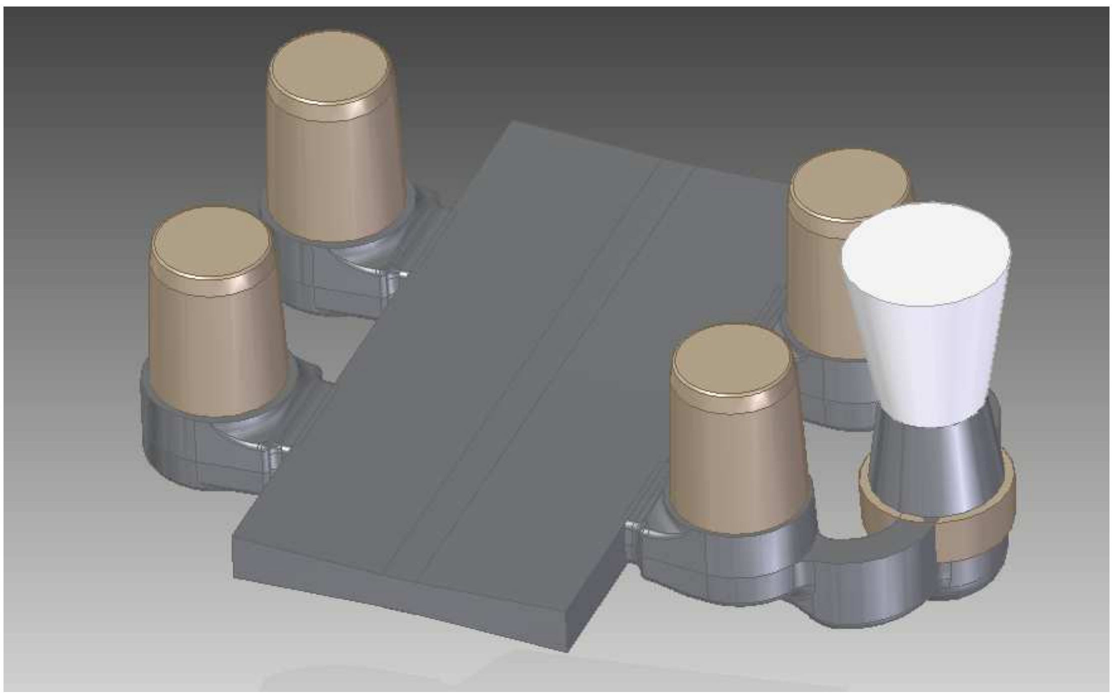

Figure 4: Cast plate riser, sprue, and gating configuration

**Nondestructive Evaluation**

Cast plates were each individually inspected using comparator plates, radiography, laser scanning, and wet magnetic particle inspection (MPI). NDE results were used to identify areas of interest within test plates. Areas of interest include casting indications that were thought to be potential fatigue crack initiation sites, such as porosity, cracks, or inclusions. Results were also utilized to evaluate how NDE may be used to predict fatigue life.

Radiography was conducted by Element Materials Technology. Results were used to identify internal porosity in cast plates.

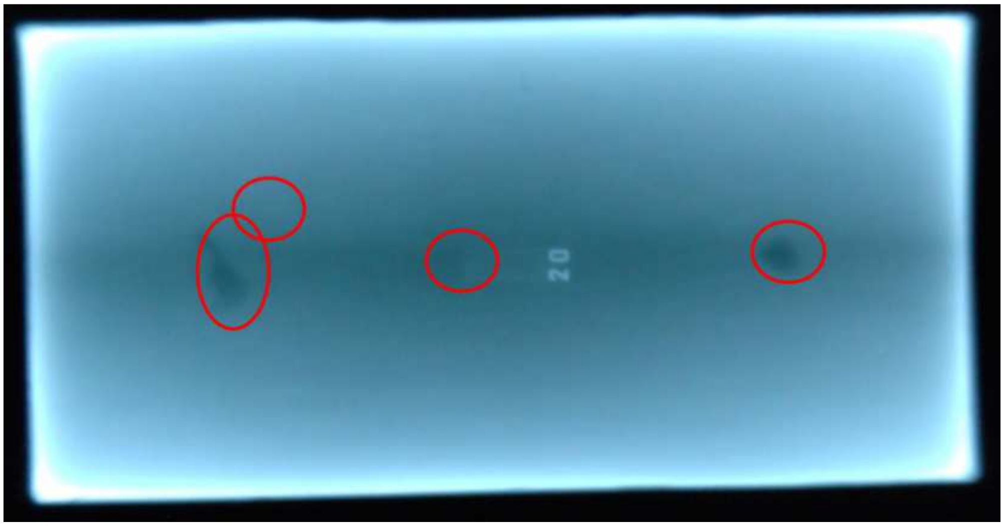

Figure 5: Radiograph with areas of interest identified

Wet magnetic particle inspection was conducted at Iowa State’s Center for Nondestructive Evaluation using a Magnaflux test bench. MPI was utilized to identify surface and near-surface indications on cast bars. A magnetic field was induced into steel plates using half-wave rectified AC at 2,200 A, to improve the test’s ability to detect near-surface indications such as porosity. 2,200A was selected to provide adequate field density and particle mobility. The test bench was prepared in accordance with ASTM E3024 [42]. Plates were inspected in two different orientations to find cracks that may be running parallel with or perpendicular to the length of each cast plate.

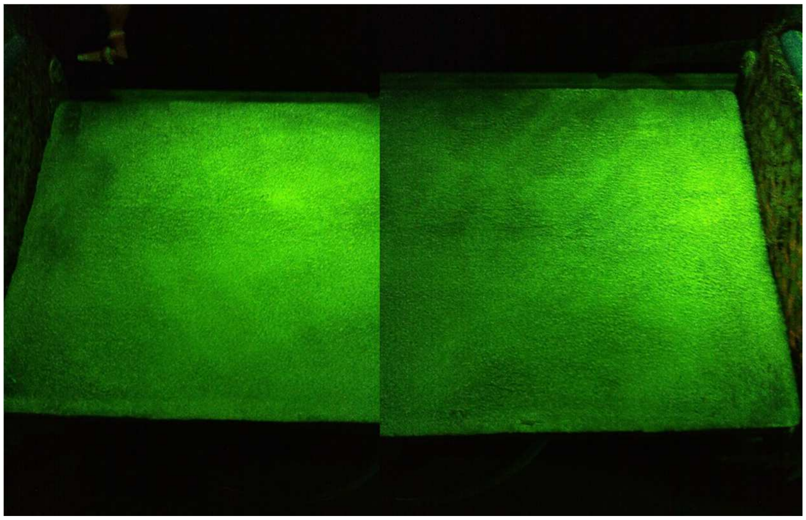

Figure 6: Magnetic particle inspection image

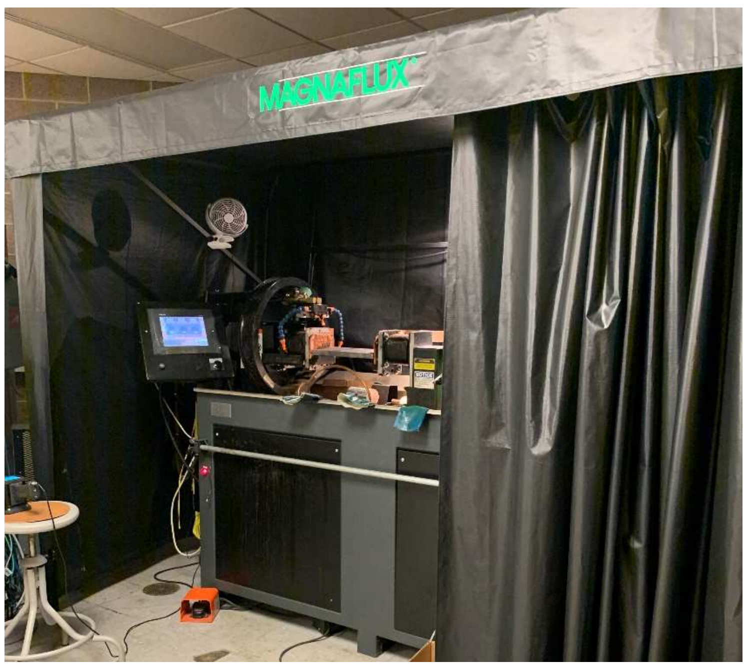


Figure 7: Magnaflux wet MPI bench

Cast surface evaluation was done through visual inspection with comparator plates, and laser scanning. ASTM A802 A-plates were used as the standard for evaluating cast surface texture. Laser scanning was conducted using a FARO laser scanner. Through laser scanning, point clouds of all cast surfaces were collected. All point clouds were then evaluated through the

Variogram Roughness Method [22] to classify cast surfaces and to compare with fatigue results. The Variogram Roughness Method provides a roughness average for an analyzed surface, as opposed to categorical classifications provided through the other surface classification technique used in this study.

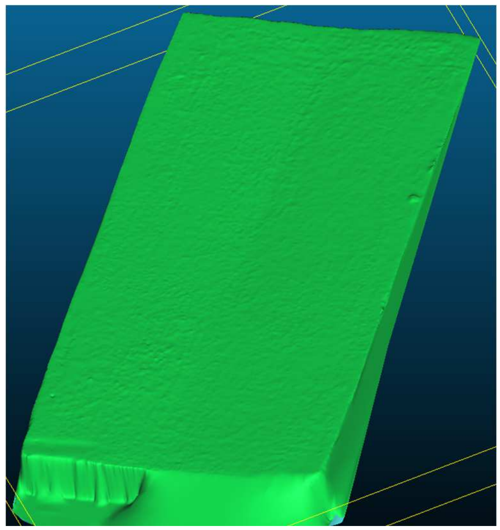

Figure 8: Surface mesh from laser scanning

### Fatigue Specimen Cutting

Test bars (Figure 9) were designed according to ASTM E466 specifications for stress concentration in the gauge area, which specifies that the radius of curvature should not be less than eight times the minimum diameter of the gauge area [43]. After test specimen locations were identified on a plate (Figure 10), they were cut via waterjet. Due to the thickness of the plates (1 inch), ridges were unintentionally created by the waterjet on the sides of test specimens, as shown in Figure 11. Due to variability in the waterjet surface roughness and to minimize the potential impact on fatigue results, the waterjet surface was removed on the final eight specimens. To remove the waterjet surface, the cut test bar radii were increased by $\frac{1}{8}$ inches, waterjet, and then machined down to the original dimensions. Machining was conducted with a

CNC Haas Mini Mill. The test bar radii were machined with a $\frac{3}{4}$ inch high speed steel end mill, with spindle speed and feed rate setpoints at 1069rpm and 6.4 inches per minute, respectively. CNC programs were developed through MasterCAM and run at 50% or less of the calculated feed rate so the program could be monitored for collisions. Additionally, all test specimen grip sections were face milled to ensure adequate clamp alignment and grip during fatigue tests (Figure 12). This was required due to the taper of the cast plates the test specimens were cut from since the grips would have the same taper if not machined. A final fatigue specimen is shown in Figure 13.

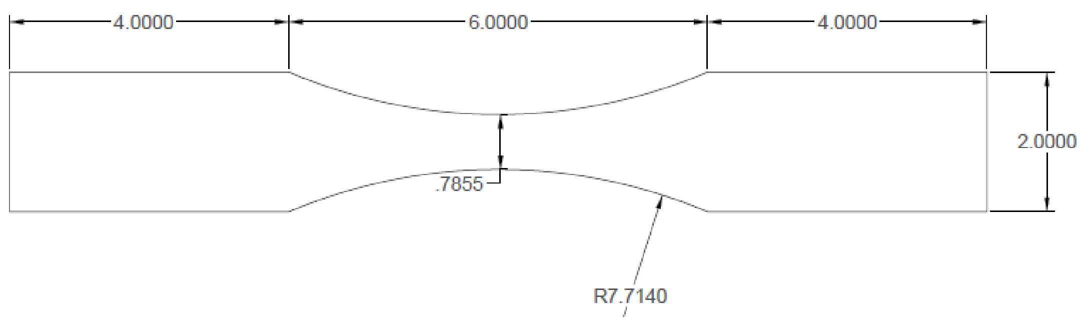


Figure 9: Dimensioned test specimen (inches)

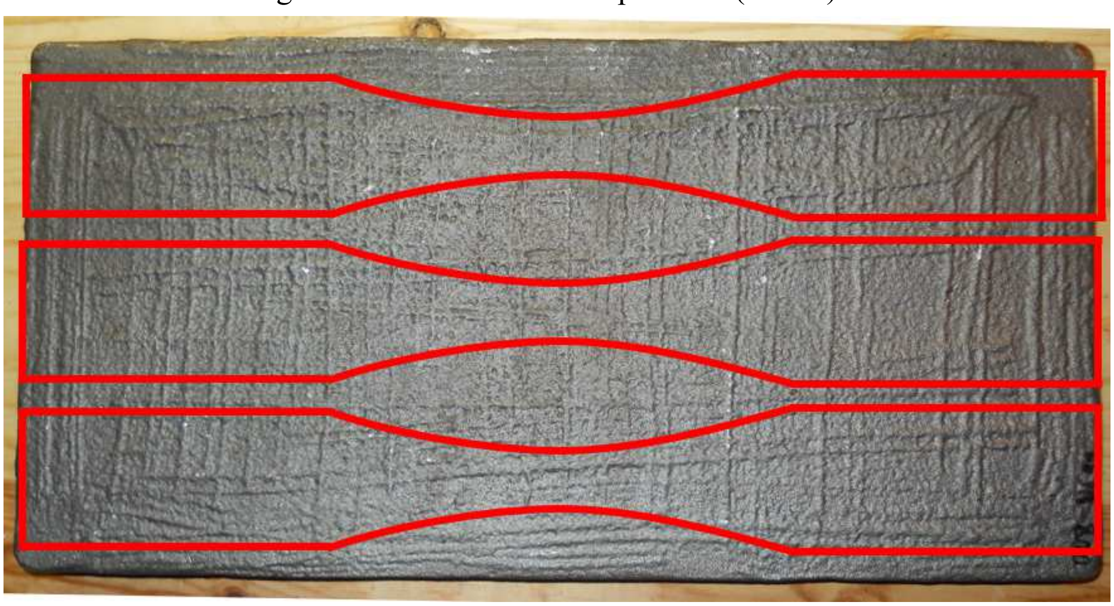

Figure 10: Cast plate with the locations of three test bars identified

Figure 11: Waterjet ridges on the side of a test specimen

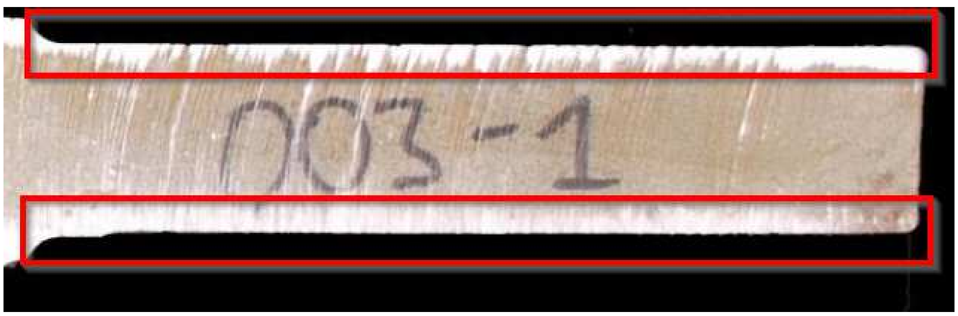


Figure 12: Side view of a machined specimen grip area, machined sections are highlighted

Figure 13: Final fatigue specimen, with grip sections and contour machined

Up to three test bars were located on each plate to capture areas of interest (Figure 10), identified through NDE. Target indications for each NDE method are described below. Areas of interest were identified to compare the severity of different indications and cast surface roughness with respect to fatigue performance. In plates with no clear areas of interest, or areas of interest that could not be captured within the test area, three equally spaced test specimens were extracted. Specimen naming followed the convention: [plate#]_[bar#]. For example, 004-3 is the third bar cut from plate four. This naming convention was used for ease of identification based on plates because manufacturing information was tied to each plate.

## Fatigue Testing

After specimens had been extracted and processed, they were fatigue tested. Axial fatigue tests were conducted on all specimens in this study. Axial fatigue, as opposed to bending fatigue, has no central loading axis where the stresses would be zero. This allows for a more balanced evaluation of surface and interior characteristics of the casting, to determine fatigue life sensitivity to multiple factors including surface finish. Stresses for indications at any point in the test specimen can be calculated easier in axial fatigue, where specimens will undergo both compressive and tensile stress.

All fatigue tests were conducted with a load ratio, R, of 0, meaning that the set tensile load was applied and then released to return to zero. This load ratio also results in a mean tensile stress. Although a mean tensile stress is known to decrease fatigue life [5], this may be more representative of product applications since many parts will undergo a mean stress. Additionally, testing with a mean tensile stress will allow for some factor of safety to be included in the generalized results, as compressive mean stresses typically increase the life of a component. Fatigue tests were conducted using an MTS 810 servohydraulic test frame with a FlexTest GT controller running Multi-Purpose Testware (MPT). Tests were conducted at 10 Hz, with fully tensile loading at 75% of tensile yield stress based on the material properties described above. This percentage was selected based on preliminary tests to give fatigue lives around $10^6$ cycles. Since fatigue at shorter lives is driven primarily by crack propagation [34] and more time is spent at the crack initiation phase at high fatigue lives, high cycle fatigue may provide a good indication as to whether or not fatigue crack nucleation is more likely to occur at a casting surface as opposed to other indications or casting features. A pilot test was conducted with strain gages placed on both sides of the specimen's gage length to ensure that there was no cyclic plasticity or unequal loading. Additionally, testing was conducted within the yield strength and elastic range of the material to avoid failures due to strain through plastic deformation. The testing process was as follows:

1. Test bar is installed into the top grips of the fatigue tester
2. The bottom of the specimen is gripped and aligned with the top grips
3. Bottom grips are clamped at zero load, to avoid preloading the specimen
4. Fatigue test is started, with a gradual ramp to the desired load

All tests were conducted until failure or until two-million cycles were reached. Any specimens reaching or failing beyond two-million cycles were considered to have too small of indications to initiate fatigue within the life of a cast part.

## Failure Analysis

Analysis of failed cross sections was conducted at the University of Alabama at Birmingham. Failure mode, initiation site area, initiation site distance along the sample edge, maximum distance between initiation site and sample edge, and maximum cluster initiation site cluster length were all measured for failed specimens. Regression analysis using linear models based on log-log transformed data were used to compare these measurements with resulting fatigue lives. One-way ANOVA was conducted to compare the fatigue lives of categorical variables such as surface classification and failure mode.

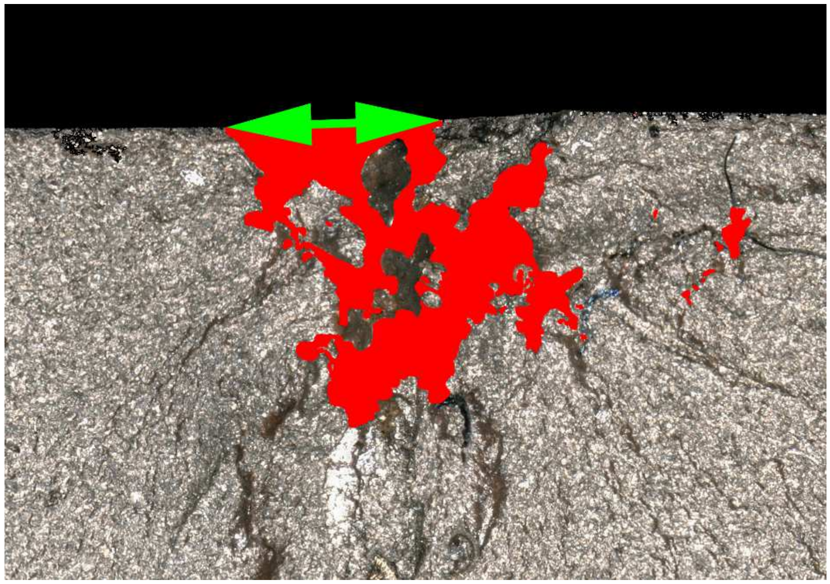

Figure 14: Initiation site distance along a sample edge, the green arrow represents the measurement

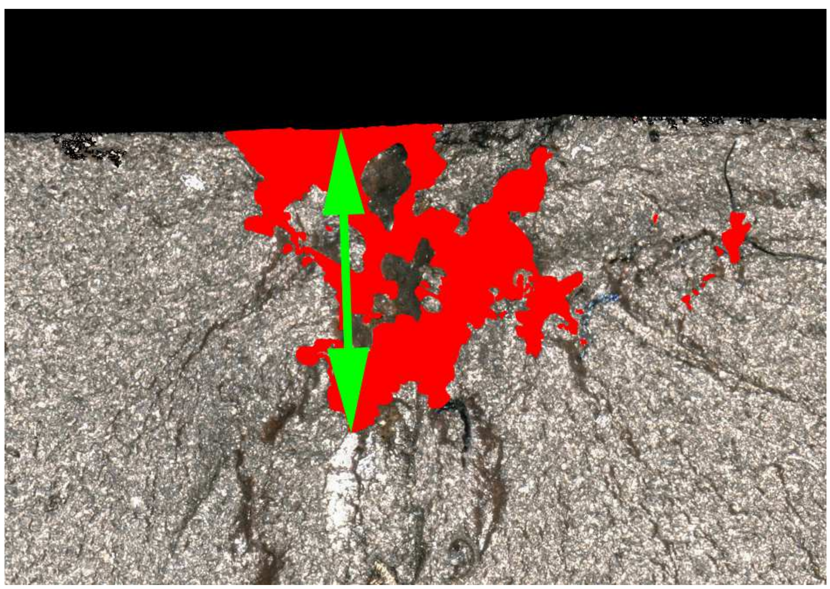

Figure 15: Maximum distance between the initiation site and specimen edge, the green arrow represents the measurement

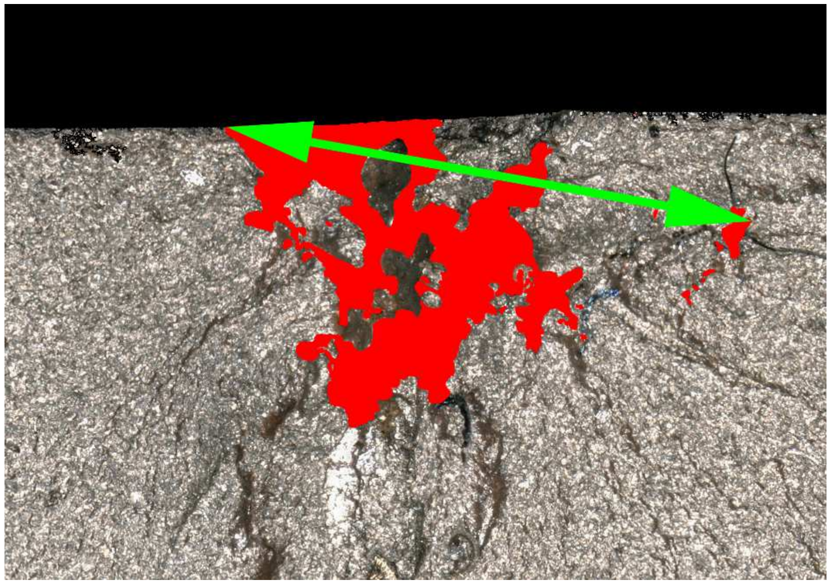

Figure 16: Maximum initiation site cluster length, the green arrow represents the measurement

# CHAPTER 3. RESULTS

All fatigue results and applied statistical analysis are presented in this section. They are organized to address the goals of this research:

1. Develop a process to explore the impact of cast surfaces with common industry classifications on fatigue life
2. Compare the influence of surface condition with porosity and other indications on fatigue life
3. Utilize nondestructive evaluation (NDE) techniques to inspect test specimens and relate results to fatigue results

The resulting stress-life curve of all tests is shown below in Figure 17.

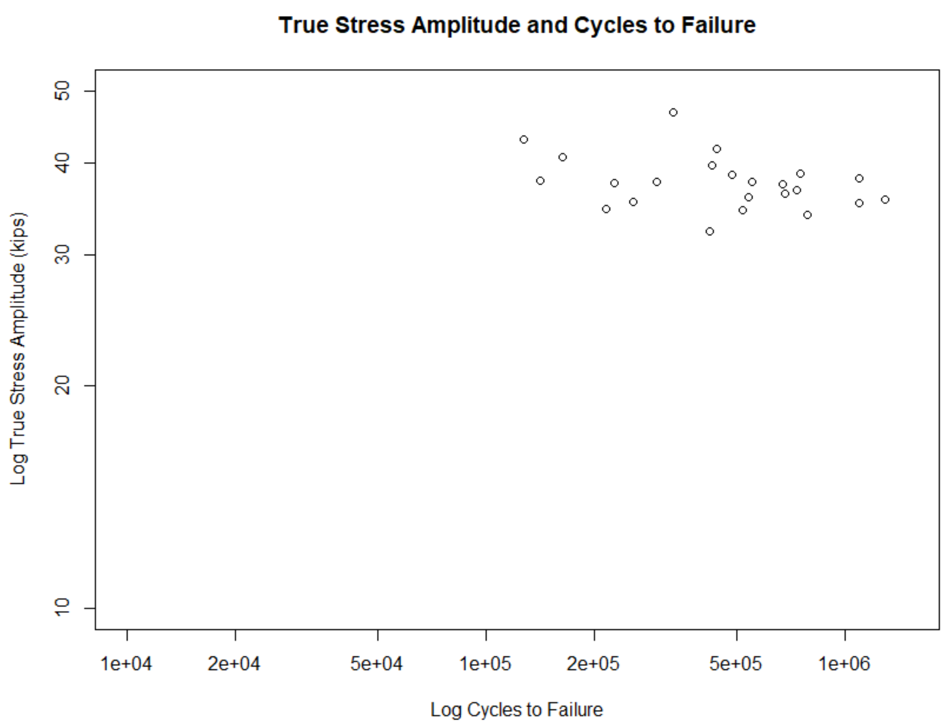


Figure 17: True stress-life curve for all samples

A breakdown of all visually classified surfaces is shown below in Figure 18. Within this study, twelve specimens failed due to cracks initiating from a cast surface, with the majority being due to indications not related to cast surface texture. The remainder of the specimens failed due to other indications internally or on non-cast sides of test specimens. This figure includes all tested specimens, even those that did not have fatigue cracks initiating from the surface. The boxplot in Figure 19 shows the cycles to failure by surface classification for specimens failing due to surface-initiating fatigue cracks. One-way ANOVA was conducted on these results, assuming equal variance shown in Table 3 and with α=0.05. No statistically significant difference in mean fatigue lives between different visual surface classifications was detected. All failures, including those not failing due to surface-initiating fatigue cracks (including surface texture, gas porosity, or other surface indications), and their associated surface classifications are shown in Figure 20. This boxplot shows one specimen that was machined on all sides, to test the variability of fatigue lives. No ANOVA was conducted on these groups, due to a large portion of failures resulting from cracks not initiating at the surface.

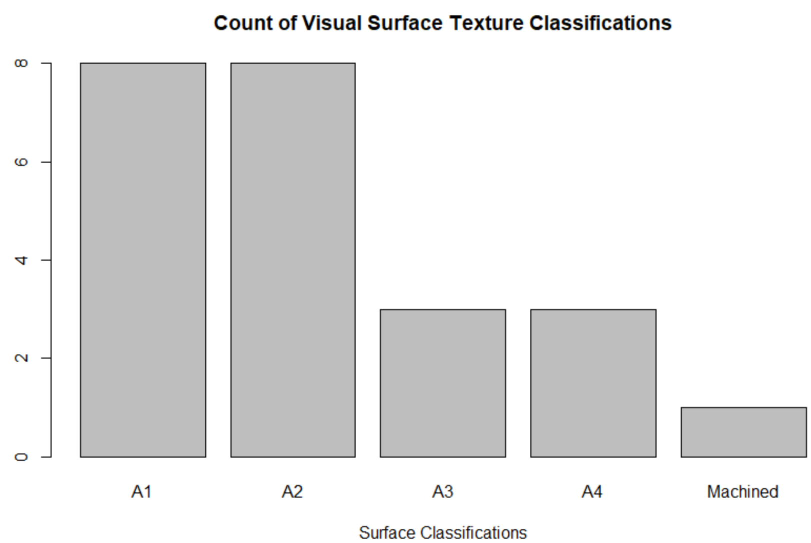


Figure 18: Count of all visual surface classifications

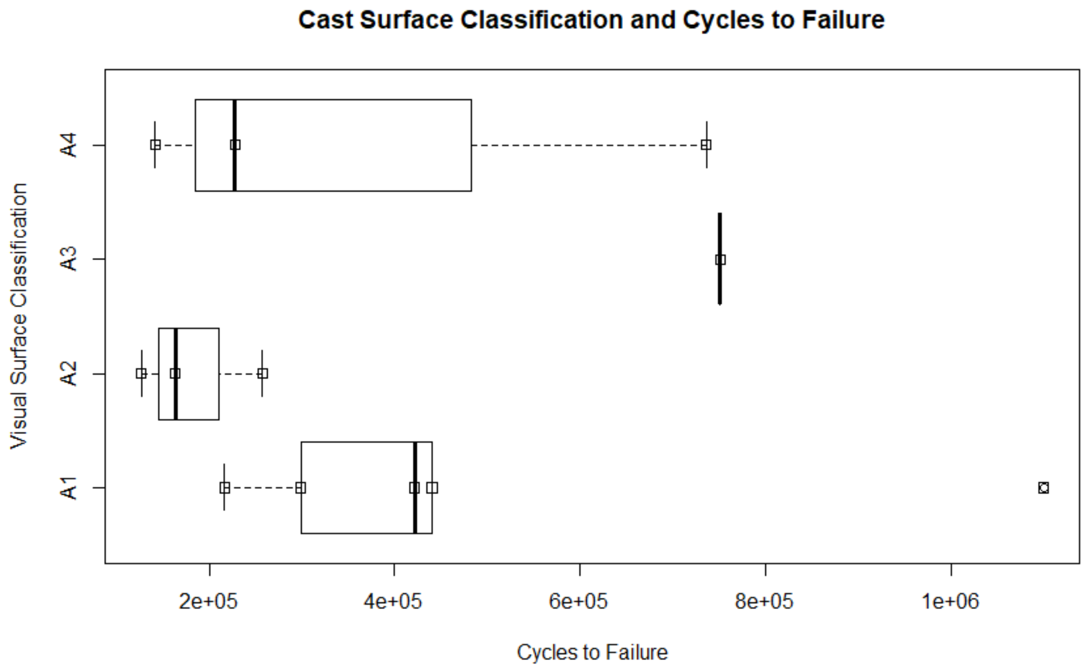


Figure 19: Cycles to failure by least rough (A1) to rough (A4) surface texture classifications per ASTM A802 [44], for specimens failing due to surface initiating fatigue cracks

Table 3: One-way ANOVA results for comparison of mean cycle lives between surface texture classifications (surface initiating failures only)

| | DF | SSE | MSE | F | P-value |
|---|---|---|---|---|---|
| Surface Classification | 3 | $3.127 \times 10^{11}$ | $1.042 \times 10^{11}$ | 1.182 | 0.376 |
| Error | 8 | $8.052 \times 10^{12}$ | $8.815 \times 10^{10}$ | | |

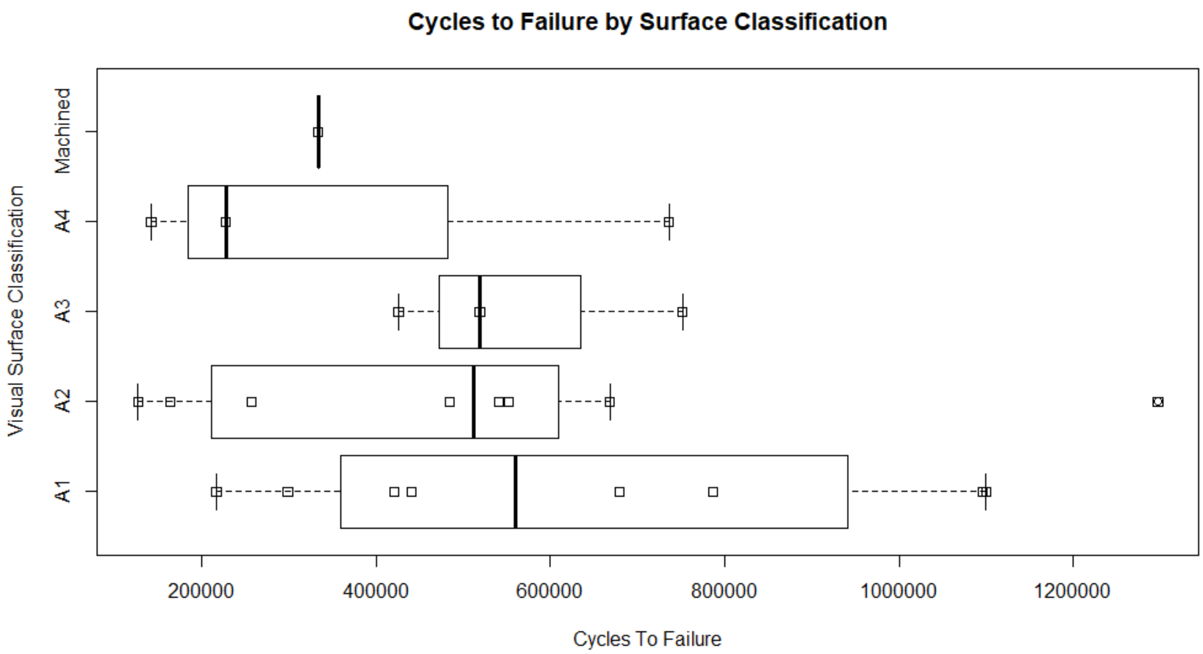


Figure 20: All failures by ASTM A802 [44] surface texture classification, with machined being the least rough, followed by A1, A2, A3, and A4

Cast surfaces were also evaluated utilizing the Variogram method [22] and laser scanning. A distribution of all Variogram cope and drag measurements are shown below in Figure 21 and Figure 22. Fatigue lives by Variogram measurements are plotted in Figure 23 for samples that failed due to surface initiating cracks, which, as stated previously, includes failures due to surface texture and surface indications such as gas porosity. Variogram measurements in this plot are from the side of crack initiation. These results show no relationship between fatigue life and Variogram surface characterization.

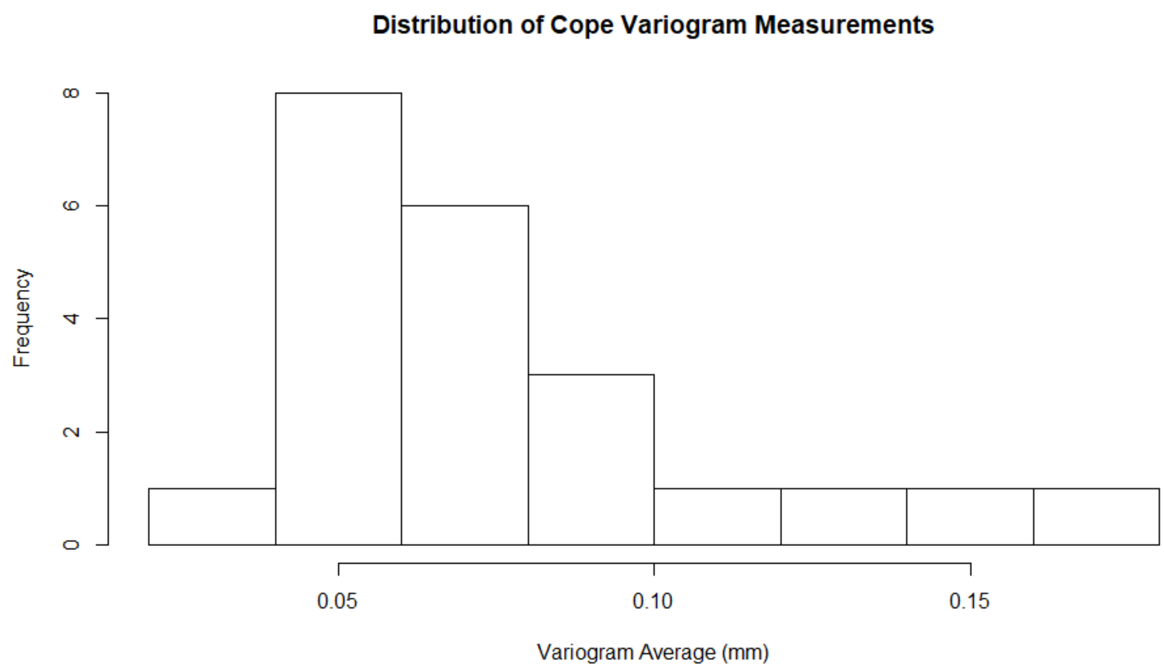


Figure 21: Distribution of cope Variogram measurements

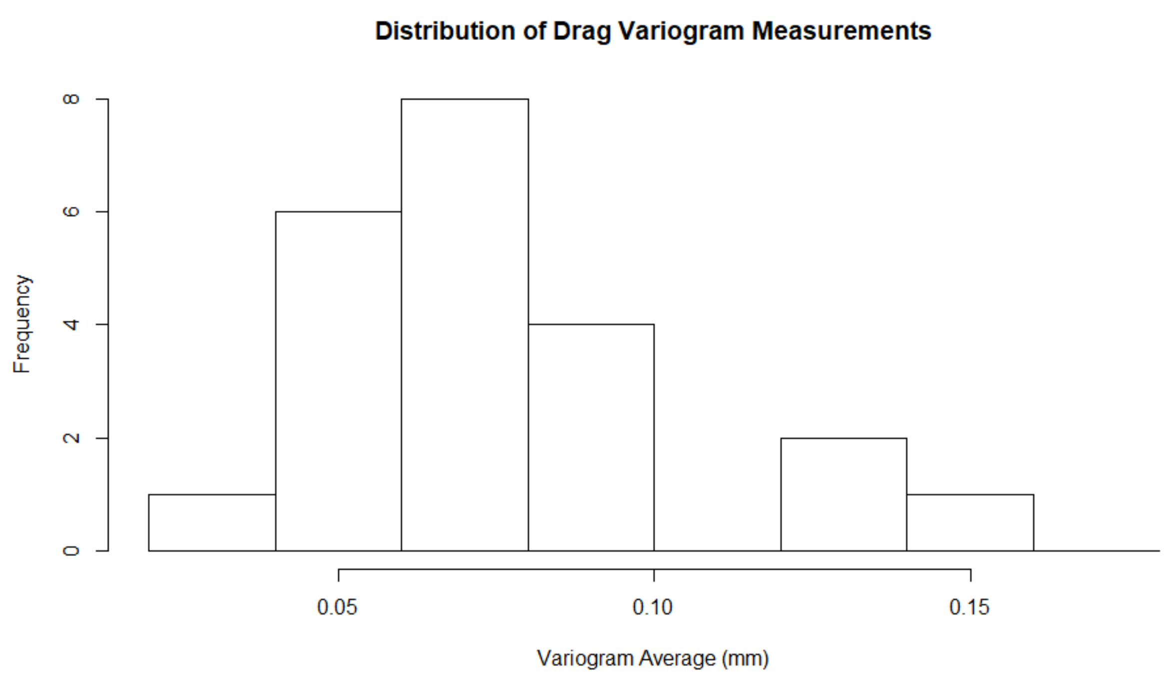


Figure 22: Distribution of drag Variogram measurements

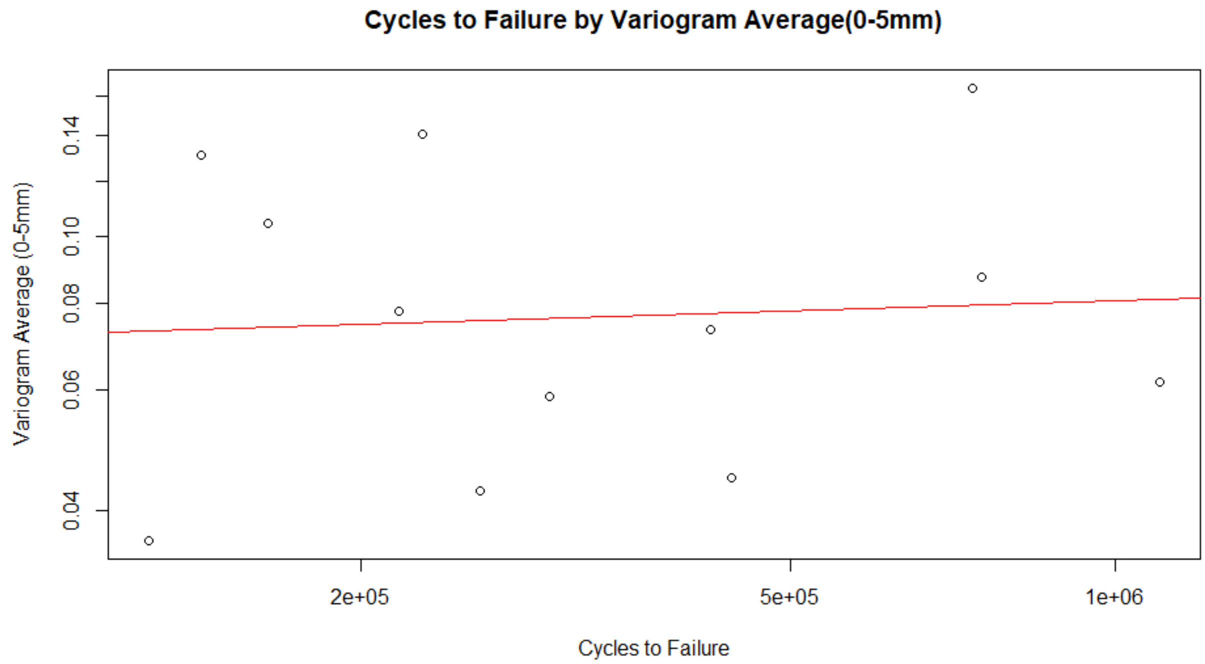


Figure 23: Cycles to failure by Variogram average for specimens with surface-initiating fatigue cracks

$Log(N_f) = 5.6208 + 0.1005 Log(variogram)$ F-statistic: 0.05006 p-value: 0.8275

Fatigue results were also grouped by fatigue initiation sites, as outlined in Table 4. A boxplot of fatigue results plotted by fatigue crack initiation site (as identified by UAB) is shown below in Figure 24. One-way ANOVA was also conducted on these results shown in Table 5, which also shows no statistically significant difference in mean fatigue lives between all six observed fatigue crack initiation sites. As shown in this figure, the largest cause of fatigue failure was centerline shrinkage. Failures due to centerline shrinkage porosity exposed on non-cast surfaces made up the largest group (Figure 25). Five failures occurred due to both shrinkage and gas porosity (Figure 26), with only two failures occurring due to non-exposed centerline shrinkage (Figure 27). Two failures occurred due to indications created through processing

(Figure 28). Gas porosity extending to the cast surface (Figure 29) was the second largest group of failures with six. Only one failure was due to cast surface texture (Figure 30).

Table 4: Initiation site code definitions

| Failure Code | Initiation Site |
|---|---|
| SSH (Figure 25) | Shrinkage porosity exposed on side (not cast) surface |
| SHG (Figure 26) | Shrinkage and gas porosity |
| SH (Figure 27) | Shrinkage porosity |
| PR (Figure 28) | Processing Defect (waterjet marks, stamp marks) |
| CSG (Figure 29) | Gas porosity extending to cast surface |
| CS (Figure 30) | Cast surface, from underlying surface roughness |

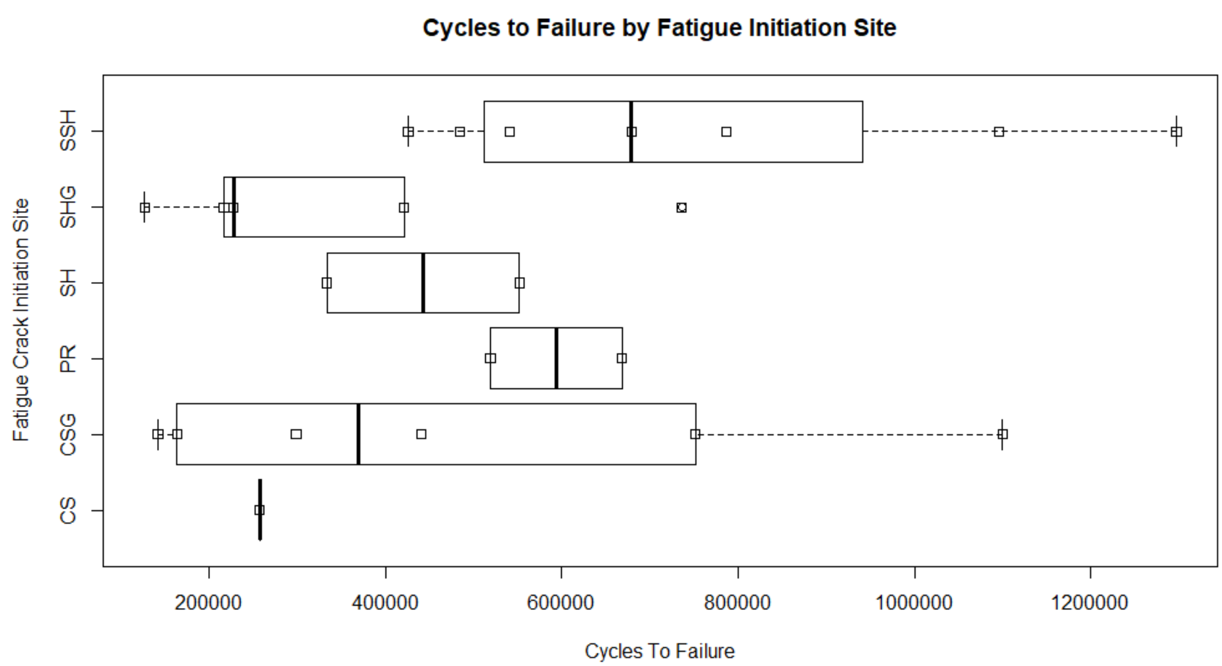


Figure 24: Cycles to failure by fatigue initiation site group for all fatigue failures

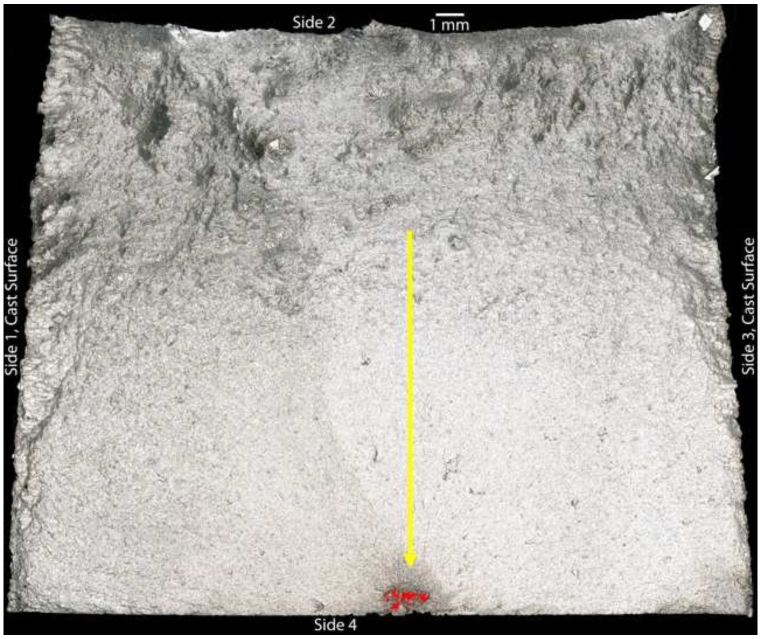


Figure 25: Cross section of a specimen that failed due to side surface shrinkage (SSH), red highlighting indicates centerline shrinkage porosity

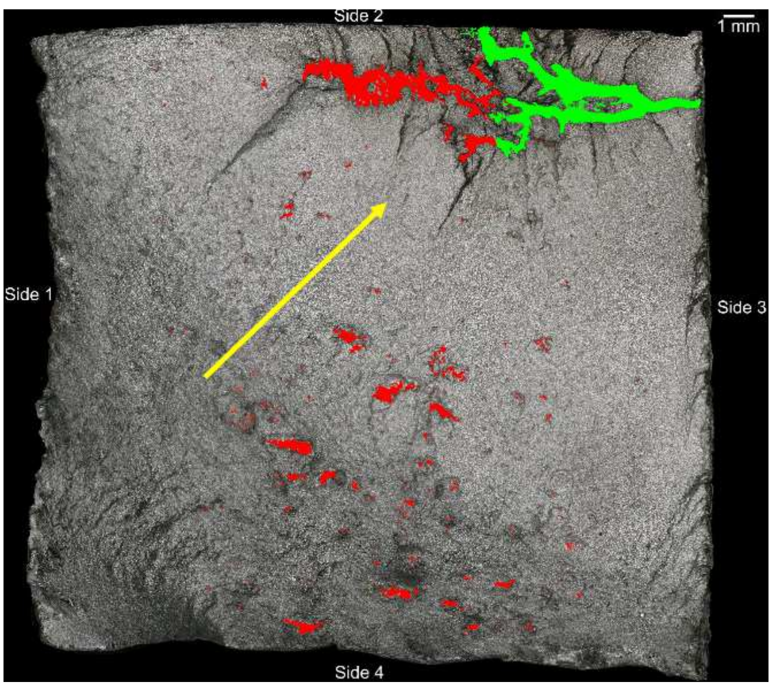


Figure 26: Cross section of a specimen that failed due to shrinkage and gas porosity (SHG), green highlighting indicates gas porosity, red indicates centerline shrinkage porosity. Top and bottom sides are cut, left is drag, right is cope.

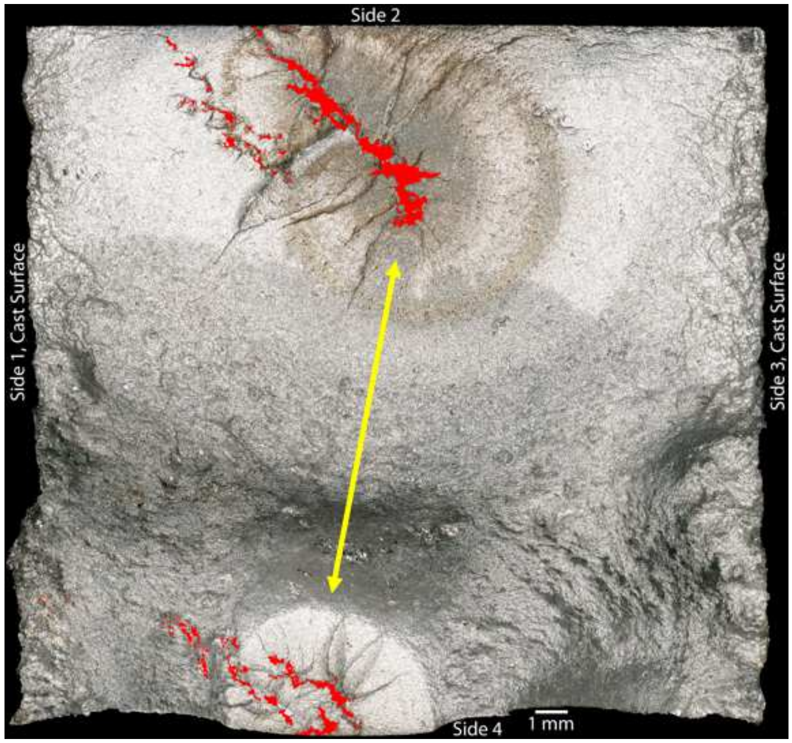


Figure 27: Cross section of a specimen that failed due to centerline shrinkage porosity (SH), red highlighting indicates centerline shrinkage porosity

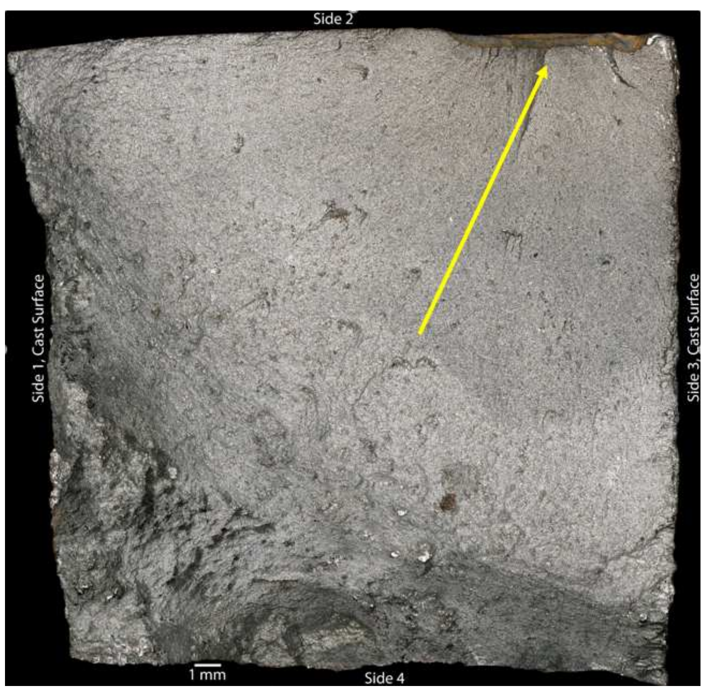


Figure 28: Cross section of a specimen that failed due to an indication created through processing; this example is a waterjet notch (PR)

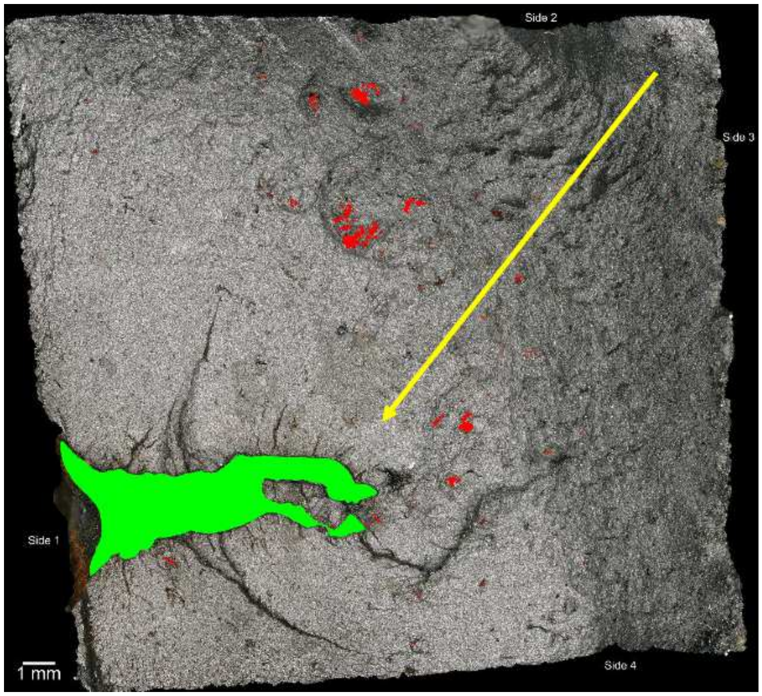


Figure 29: Cross section of a specimen that failed due gas porosity extending to the cast surface (CSG), green highlighting indicates gas porosity, red indicates centerline shrinkage porosity. Top and bottom are cut sides, left is cope, right is drag.

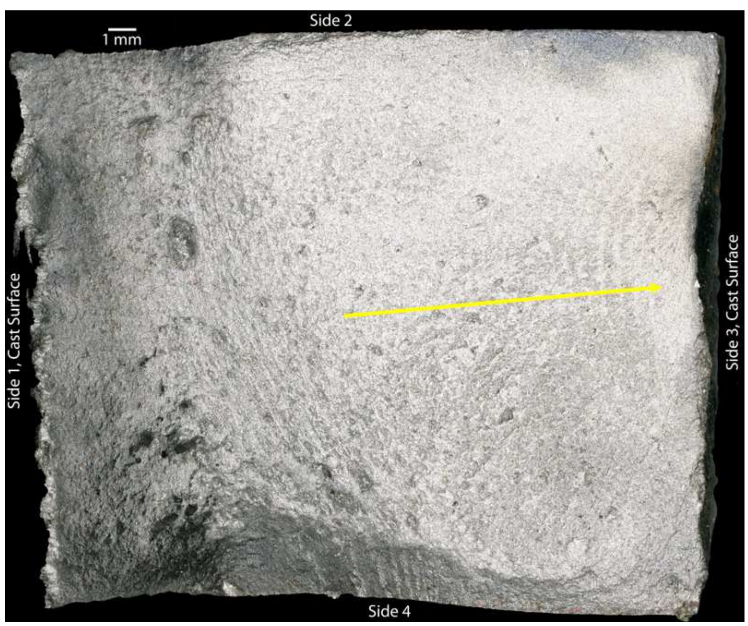


Figure 30: Cross section of a specimen that failed due to the cast surface (CS). The right side is cope, left side is drag.

Table 5: One-way ANOVA results comparing mean fatigue lives between fatigue crack initiation reasons

| | DF | SSE | MSE | F | P-value |
|---|---|---|---|---|---|
| Failure Reason | 5 | $6.452 \times 10^{11}$ | $1.290 \times 10^{11}$ | 1.353 | 0.29 |
| Error | 17 | $1.621 \times 10^{12}$ | $9.536 \times 10^{10}$ | | |

Physical measurements of failure cross sections were measured by UAB and analyzed by feature length, cluster length (Figure 16), and $\sqrt{initiation\ site\ area}$ based on the Paris Law of fatigue crack growth. Feature length was determined by using the maximum of either the feature length along the edge (Figure 14) or feature length from the edge (Figure 15) for surface initiation sites, or diameter for internal initiation sites. The $\sqrt{area}$ method was used since it has been shown to be a reasonable size estimate for irregular crack shapes [36]. Linear models of log-log plots were developed to form a characteristic curve for this material. Even with our high fatigue life variability, these models were all statistically significant. This indicates that major variation in fatigue lives can be accounted for through log-log regressions of initiation site measurements. Initiation site areas were unable to be measured on some specimens, leading to reduced degrees of freedom in the $\sqrt{initiation\ site\ area}$ model. For consistency to other plots in this paper, cycles to failure are plotted on the x-axis, but linear regressions for log-log plots are shown with $N_f$ as the response variable.

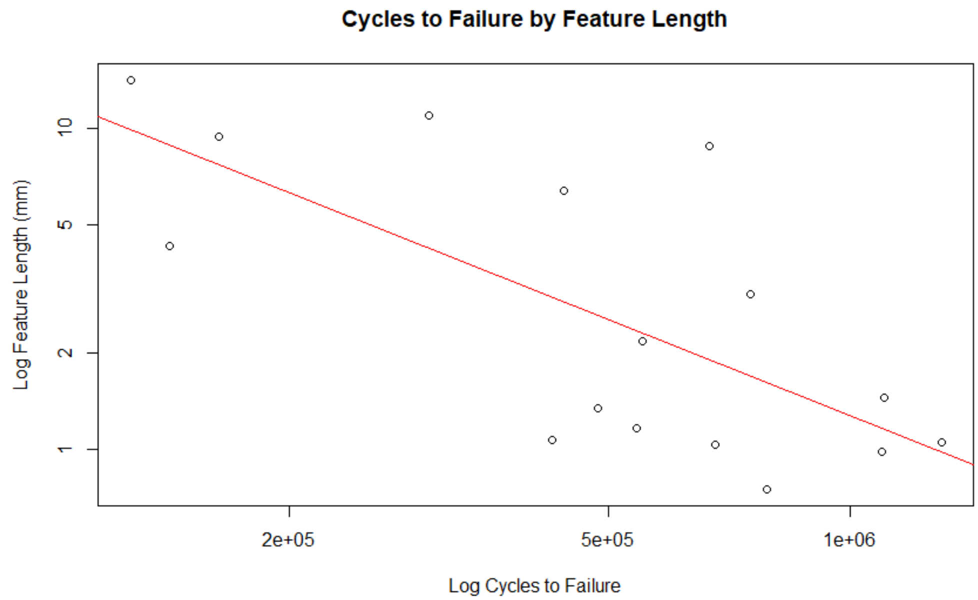


Figure 31: Log-log of cycles to failure by feature length with linear regression line

$Log(N_f) = 5.8923 - 0.4923Log(a_0)$ F-statistic: 13.5 p-value: 0.002

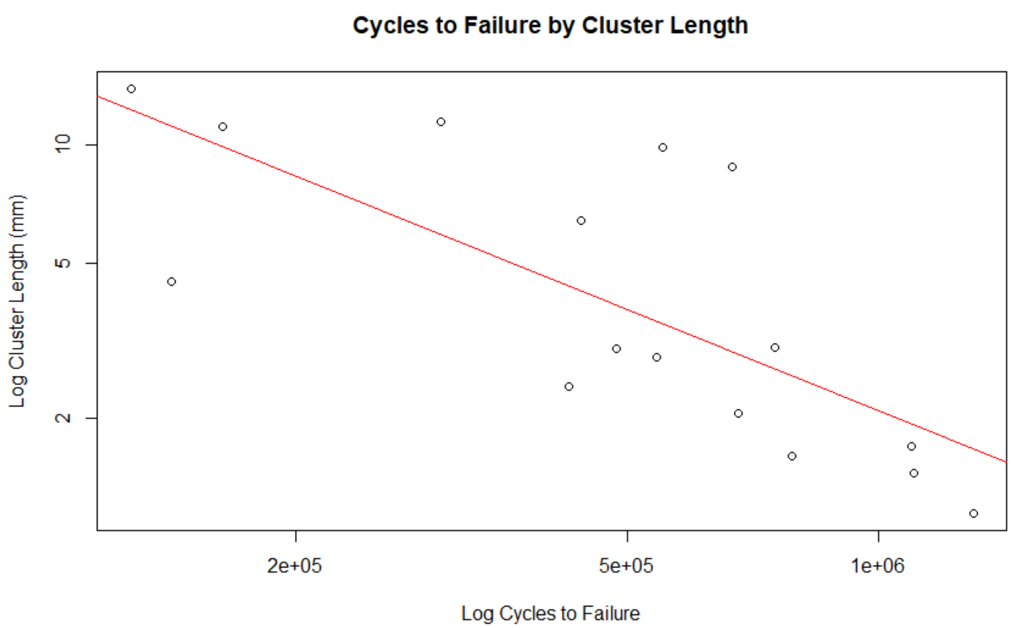


Figure 32: Log-log plot of cycles to failure by cluster length with a regression line

$Log(N_f) = 6.0603 - 0.6328Log(a_0)$ F-statistic: 16.59 p-value: 0.001

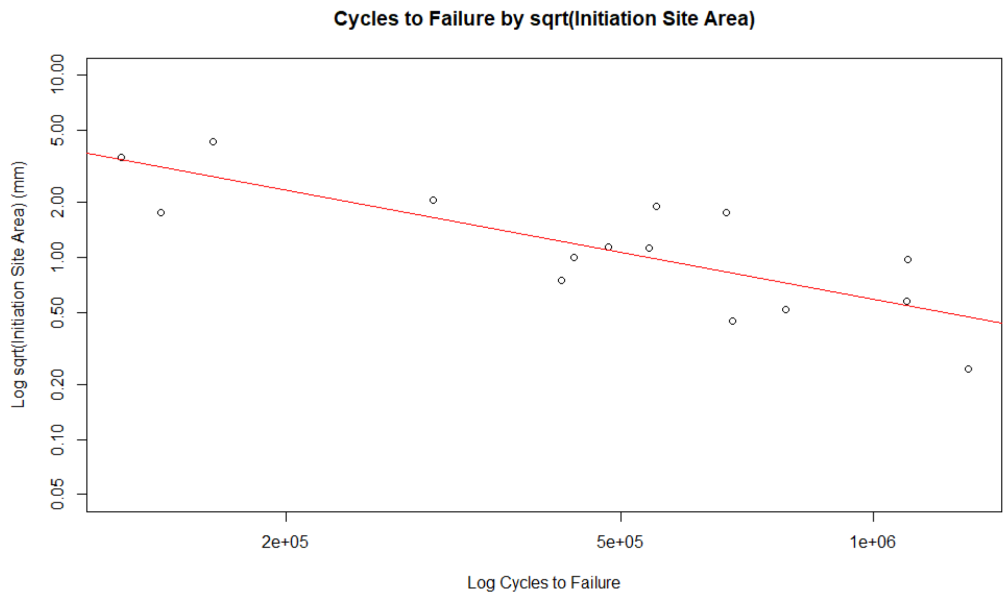


Figure 33: Log-log plot of cycles to failure by $\sqrt{area}$ with regression line

$Log(N_f) = 5.7127 - 0.7448Log(a_0)$ F-statistic: 22.76 p-value: <0.001

# CHAPTER 4. DISCUSSION

This chapter includes a discussion of the results presented above and their relation to related studies and previous knowledge. There are three sections in this chapter, each discussing the research goals outlined in Chapter 1: testing process development, fatigue testing results as they relate to surface condition, and potential use of NDE to determine fatigue performance.

## Process Development and Results

As indicated in Chapter 1, little work has been done to investigate the level of influence cast surface condition has on fatigue performance. The testing process developed through this research was intended to evaluate the influence of cast surface condition when compared to other common casting characteristics such as internal porosity or large surface indications. Resulting specimen testing and processing methods, as outlined in Chapter 2, were utilized to effectively evaluate the fatigue performance of cast parts.

The test specimen designed for this process was developed to focus on cast surfaces and cast features. To evaluate the extent of cast surface influence on fatigue life, cope and drag surfaces were both maintained on test specimens, with both edges being waterjet and machined. Previous research has shown that machined surfaces exhibit better fatigue life than as-cast parts [32]. With this, it was estimated that most surface failures would initiate from the cast surface instead of the waterjet and machined surfaces. Although, as shown in Figure 24, approximately the same amount of failures initiated from the side surfaces as from the cast surfaces. This was primarily due to centerline shrinkage porosity being exposed on the side surface by waterjet cutting and machining (Figure 25). To gather more cast surface failure data, centerline shrinkage will have to be minimized as it proved to be more detrimental to fatigue life than cast surface finish.

Applied loads were calculated based on specimen cross section for all tests to minimize variability caused by varying cross section measurements. The first five specimens were all tested at the same load. The procedure was then modified after those five tests to accommodate varying cross sections. As seen in Figure 17, the resulting true stress levels for all failed specimens (including the first five tests) were all effectively maintained around 75% of the yield strength, with no correlation between true stress and fatigue life. Beyond the first five tests being loaded at the same stress level, additional variability in this chart was primarily due to failures occurring at locations other than the center of the test specimen. Due to the design of the test specimen, the cross section varies from the center to the end of the gauge length, causing variability in true stress measurements. This was expected, as casting indications could occur along the entire length of the bar. As mentioned in Chapter 2, the targeted stress level was within the elastic range of the material to avoid failures due to cyclic plasticity. Avoidance of cyclic plasticity allowed for ease of comparison so that plastic strain would not need to be included in the evaluation of fatigue failures. All resulting true stresses remained within the elastic range of the material (Figure 17).

High cycle fatigue was chosen as the starting point for evaluating the influence of casting surface finish on fatigue life. To evaluate different cast surface textures, failures had to initiate from the surface. As stated in *Fundamentals of Metal Fatigue Analysis* by Bannantine et al., surface finish will have more of an impact at higher fatigue lives where more time is spent in the crack initiation phase [34]. Based on this information, testing at a load to attain lives from $10^5$ to greater than $10^6$ increased the probability of fatigue failures initiation from the surface. It is important to note that other factors such as microstructure, hardness, and ductility also influence the sensitivity of a material to surface stress concentrations.

Through axial testing, as opposed to bending, all casting characteristics between specimens can be evaluated equally with little additional calculation. For example, a gas pore will experience the same stress as the cast surface within the same cross section. This allows for the impact of those two characteristics to be easily compared. This allowed the test to identify what indications are the most influential on fatigue life. With an R ratio of 0, each specimen was tested with a mean tensile stress. As mentioned in Chapter 2, a mean tensile stress is known to decrease fatigue life, while a compressive mean stress will increase fatigue life [5]. It was also mentioned that this loading method was applied due to industry applicability. This method may also allow for a potential factor of safety in any fatigue prediction models developed through this research. For example, the regressions shown in Figure 31, Figure 32, and Figure 33 will all be predicting lives slightly shorter than expected due to the known effects of a mean stress. There are multiple methods (Goodman, Smith-Watson-Topper, etc.) that can be used to estimate the effects of a mean stress on part performance and could be applied to the predictions from the models above.

### Influence of Casting Indications and Surface Condition on Fatigue Life

As mentioned in Chapter 1, this process and research were developed to investigate the influence of different casting indications and characteristics on fatigue life. Additionally, the influence of varying casting surface roughness was also evaluated. Through the testing in this research, it was shown that fatigue failures were more likely to initiate due to gas or shrinkage porosity than due to roughness of the cast surface. Different cast surfaces did not exhibit different fatigue lives if classified through traditional visual methods or the Variogram method. Although, due to the lack of samples failing due to cast surface roughness, there is a need to investigate the differences without the presence of other indications in large test specimens.

As shown in Figure 19 and summarized in Table 3, there is no clear difference in fatigue lives between different cast surface classifications. In Figure 19 and Table 3, only specimens with cast-surface initiating failures were included in the analysis, since those are the only failures where cast surface may have interacted. All specimen fatigue lives, and their surface classifications are shown in Figure 20 to show the variety of surface classifications tested and the variability of the resulting fatigue lives. From these results, cast surface roughness as classified through visual inspection is not a reliable indicator of fatigue life.

The qualitative nature of visual inspection is difficult to correlate with a quantitative part performance attribute like fatigue life. Due to this, the Variogram method [20] [22] was also used to evaluate fatigue life based on cast surface texture. Variogram measurements for surfaces where fatigue cracks initiated from are plotted against cycles to failure in Figure 23, with distributions of cope and drag Variogram measurements shown in Figure 21 and Figure 22, respectively. It is clear through Figure 23 and the resulting linear model p-value that Variogram roughness is also not correlated with fatigue lives in specimens that failed due to surface-initiating fatigue cracks. These results also confirm that cast surface texture, in the presence of other indications, is not a reliable indicator of fatigue performance.

Potential indicators of fatigue performance were identified using measurements from the University of Alabama at Birmingham's (UAB) analysis on the failed cross sections of test specimens. Initiation feature length, cluster length, and $\sqrt{initiation\ site\ area}$ were all plotted against cycles to failure in Figure 31, Figure 32, and Figure 33, respectively. These were selected for use in the Paris equation (Equation 4) and its integrated form solving for $N_f$ (Equation 5). Under the same testing conditions and with the same material, for comparison purposes, the equation is reduced down to $\frac{1}{{a_0}^{\frac{m-2}{2}}}$ and then to $\frac{1}{a_0}$ with m being the slope of the linear region in a log-log $\frac{da}{dN} \sim \Delta K$ plot. $a_0$ is a length measurement or length estimate of the fatigue crack initiation site. As mentioned in Chapter 1 and shown in Equation 8, $\sqrt{area}$ can be substituted as a size estimate for irregular crack shapes. To compare the measurements mentioned above, log-log plots and regressions were developed to compare how each method of initiation site evaluation compared in predicting fatigue life.

Looking at the p-values and F-statistics of each regression model (Figure 31, Figure 32, and Figure 33) show that all crack length measurements used are effective estimates for $a_0$, and that use of the integrated Paris equation is useful for estimating fatigue performance of a given material. All regressions show that increasing initial initiation site measurements lead to decreased fatigue life. This is intuitive in a stress concentration sense but also proves that no matter the source of a casting indication, the most important factor is the indication size. In this research, $\sqrt{area}$ proved as the best estimate for $a_0$ (Figure 33). The regression produced by this plot gives a slope of -0.7448, and when related back to the simplified Paris equation for $a_0$, can be set equal to $-\frac{m-2}{2}$. This produces an m value of 3.49 in the Paris equation. Values for similar steels range from 3 (A216 grade WCC [30]) to 3.8 (A27 [45]), this similarity further validates the use of $\sqrt{area}$ and the integrated Paris equation as an estimate for high-cycle fatigue performance for a given material.

One note regarding this prediction method is that there is still some variability in the results. Many fatigue modeling techniques use distributions and probabilistic information to predict fatigue performance. With the variability encountered in fatigue performance in this study, relating site measurements to fatigue life is just a starting point, and that use of probabilistic information is the next step in developing the model. This development is discussed further in Chapter 5. It is also important to note that this prediction method was developed through controlled testing of large lab-scale specimens. While these are believed to be more representative of the behavior of cast parts, the loading conditions experienced by these are not representative in all applications. Cast parts may be exposed to further stresses and strains through torsion and bending. With or without an applied axial load, torsion or bending can severely impact fatigue performance. Part application and loading must still be considered when predicting part performance.

Although neither cast surface texture inspection technique indicated that surface roughness is a leading indicator of fatigue life, many failures still initiated from gas porosity on the cast surface (Figure 24). With this, characterization of these indications will be important to predict the fatigue life of cast parts. However, gas porosity does not impact surface texture classifications and is only identifiable through NDE in many cases. As shown in Figure 31 and Figure 33, fatigue life decreases with increasing initiation site size on a log-log scale. This shows that while surface roughness may not be an indicator of fatigue performance, surface quality is. If a produced surface includes multiple large indications due to gas porosity (Figure 29) or post-processing errors (Figure 28), the surface quality may influence fatigue life. Based on the results presented in the figures mentioned previously, it is expected that larger gas porosity will have a negative influence on fatigue life. However, this testing has further revealed that surface condition is not the only important factor in casting fatigue performance and that indication size is a larger contributor to varying fatigue life.

As seen in Figure 24, many failures through these tests were due to centerline shrinkage exposed on the side surface of test specimens. While they were still machined to get rid of stress concentrations created by the waterjet, shrinkage porosity was still a contributor to many of the fatigue failures through these tests. Shrinkage porosity exposed on the side surface was not identifiable through radiography in most cases and would have been considered acceptable if not exposed through specimen manufacturing. Although the shrinkage porosity exposed on the surface was very small, it still led to fatigue failure as opposed to cast surface roughness. Thus, this is another indication that initiation site size is a more important factor in fatigue life than cast surface texture.

## NDE and Fatigue Results

Another goal of this research was to identify what NDE methods may be used to effectively estimate a given cast part's fatigue performance. On five occasions, fatigue initiation sites were identified through visual inspection of test specimens. All cases were either exposed shrinkage porosity, processing indications, or large gas porosity. As mentioned in the previous section, visual surface classification and laser scanning of surface texture did not have strong connections with fatigue results. Radiographs were used to effectively identify the presence of internal shrinkage porosity for test bar locating but were difficult to use to identify a single fatigue initiation site. No indications were found through MPI. One shortcoming of the NDE conducted in this research is the qualitative nature of the data collected. For the prediction of a quantitative property like fatigue life, it is necessary to identify more quantitative indicators to use in prediction models.

Visual inspection was utilized, as in industry, to identify areas of interest in cast plates. In cases where large gas porosity, manufacturing defects, or exposed shrinkage porosity were present, visual inspection was effective at identifying fatigue crack initiation sites. As expected, any indication large enough to be identified visually typically led to fatigue failure, especially in the case of large gas porosity or manufacturing defects. Although able to identify initiation sites, the use of visual inspection could not be used to estimate the fatigue life of a part. In some cases, visually identified fatigue initiation sites on the surfaces of specimens performed better than surface indications not found through inspection. Additionally, not enough indications were found to analyze the influence of different classifications of indications on fatigue performance. Surface texture, however, was classified through visual inspection and laser scanning with the Variogram method. Neither of these methods produced any link between surface texture and fatigue failure. Most cast surface failures initiated due to gas porosity in the cast surface (Figure 29). In many cases, this porosity was too small to be found through the Variogram method or visual inspection and classification. However, due to the results based on initiation site area, future use of the Variogram method may be able to link indication values with fatigue life if individual indications can be classified using the method.

Radiography was used to identify the presence of shrinkage porosity in cast plates. Similarly, with the visual classification methods, the qualitative nature of the radiograph inspection techniques used in this research are difficult to link to potential fatigue performance of a part. Other than identifying potential fatigue crack initiation sites, the extent of the impact of indications identified through radiography is still unknown. Quantification of these indications in terms of size and shape, when related to the loading direction, could be useful in the prediction of a part’s fatigue performance. Many fatigue failures due to centerline shrinkage were too small to be identified through radiographs. Microporosity still needs to be considered when evaluating cast part performance, especially in parts with no other indications. One note from this research is that most failures due to internal centerline shrinkage were exposed on the machined sides of test specimens. Further evaluation of internal versus external indications is needed due to the lack of failures due to internal features only in this research.

No indications were found through MPI for specimens tested in this research, beyond those already identifiable through visual inspection. Due to the casting and specimen design, surface cracks due to hot tears that would be identifiable through MPI were not a factor. Additionally, cast surface roughness hindered particle flow over the plates, which would make it difficult to identify small surface or subsurface indications. Cast surface roughness also may have made it too difficult to differentiate small surface or sub-surface gas porosity from surface roughness.

Only axial fatigue was conducted in this study, the impact of torsion or bending forces could change a part's sensitivity to different types of indications. As a result, the appropriateness of each NDE technique and their results for the evaluation of part performance may vary based on part application and loading. Future development of these methods is discussed further in Chapter 5.

# CHAPTER 5. CONCLUSIONS AND FUTURE WORK

Through this thesis, a process of cast fatigue specimen manufacturing, inspection, processing, and testing has been developed. Additionally, results have been provided proving the viability of this testing process for the evaluation of cast surface condition and its influence on fatigue performance in the presence of other casting indications. NDE was used to inspect test specimens to investigate the potential to predict fatigue performance through their results. Resulting fatigue tests also provided an idea of what indications are most likely to impact long-term fatigue performance in large cast parts, leading to a better understanding of what to look for through NDE. Finally, regressions were developed for this material using the integrated Paris law to identify what features of an indication describe the largest amount of variability in fatigue performance.

## Conclusions

This study investigated the influence of varying cast surface condition on fatigue life. As seen in Figure 19 and Figure 23, both qualitative and quantitative surface evaluation techniques show little relation between cast surface texture classification and fatigue performance. The qualitative inspection technique showed no relation between surface classification and fatigue life with an ANOVA p-value of 0.376. A linear model using log cycles to failure and log Variogram average produced a p-value of 0.8275. This evaluation was intentionally conducted in the presence of other casting indications like interior porosity, and unintentionally through processing defects like waterjet ridges. When these indications are present, long-term cast part failures are more likely to occur due to initiation sites other than surface roughness as seen in Figure 24. An ANOVA of fatigue initiation sites shows no statistically significant difference in fatigue life between failure initiation sites (p-value: 0.29). Additionally, most failures initiated from surface indications, either through gas porosity on cast surfaces or through centerline shrinkage exposed on machined surfaces. Further analysis of failed specimens identified that the use of initiation site lengths, either measured or estimated from the $\sqrt{area}$ method, and use of a reduced Paris Law provided reliable estimates for fatigue lives of a given material, as seen in Figure 31, Figure 32, and Figure 33 (p-values: 0.002, 0.001, and <0.001, respectively). This also shows that a cast parts fatigue performance is more sensitive to indication size than how it was formed (gas or shrinkage porosity, surface roughness, etc.).

In some cases, NDE was able to identify fatigue crack initiation sites before testing, primarily through visual inspection. In radiographs, interior porosity was identified as a potential fatigue crack initiation site before some specimens were processed and tested. In other cases, interior porosity caused failures but was not identifiable through radiographs. Visual inspection was used to identify surface fatigue crack initiation sites in the form of large gas porosity, exposed centerline shrinkage, or processing notches. Through radiographs or visual inspection, potential initiation sites could be identified but the magnitude of their impact could not be evaluated due to the qualitative nature of the fatigue results. Using the Variogram method proved as a useful tool to quantify surface condition but did not provide a link to fatigue performance. No indications were found through MPI, so those results were not able to be evaluated with fatigue performance.

## Limitations and Future Work

Many limitations were identified through specimen manufacturing, processing, testing, and results analysis. One of the primary limitations of this study was the lack of failures due to cast surface roughness. Even though resulting fatigue tests were useful in identifying the impact of cast surface roughness on fatigue life relative to other indications, the lack of surface roughness initiation fatigue cracks did not allow for definitive comparisons between surface classifications. Another limitation was the number of failures due to unintentional indications, like processing defects and exposed centerline shrinkage. These indications proved to be more impactful to fatigue life than surface indications or interior shrinkage porosity in many cases and added to the variability of the study. The lack of quantifiable data in NDE techniques also limited the ability to relate fatigue performance with NDE results. Though some methods proved useful to identify initiation sites, the magnitude of impact was not able to be identified through preliminary inspection.

Addressing many of these limitations composes most of the future work relating to this research. One primary focus of future work should be to better quantify NDE results. Through the relation of initiation site size to fatigue life as identified in this study, there is potential for the use of NDE methods like radiography, MPI, and surface scanning to be used to estimate fatigue performance of cast parts.

Other primary focuses of future work should include developing testing methods to evaluate cast surface condition alone in large parts and eliminate surface-exposed centerline shrinkage porosity. Through the results of this study, cast specimens were more likely to fail due to reasons other than cast surface texture. However, due to having only one failure due to cast surface texture, relationships between different classifications and resulting fatigue lives could not be developed. Elimination of exposed centerline will allow for an evaluation of fatigue performance as it relates to primarily cast characteristics, rather than those due to specimen manufacturing and processing. Finally, many more samples will need to be tested from this material and other materials to validate the analysis and fatigue prediction methods utilized and proposed through this research.

Another part of the proposed future work stemming from this research is the integration of probabilistic techniques with the fatigue life prediction methods in this research. As discussed in both Chapter 1 and Chapter 4, some methods that use probabilistic information to infer fatigue lives. With the variability in both NDE techniques and fatigue performance, it may be reasonable to develop the model used in this further to include probabilistic information. For example, probabilities of estimated initiation site areas could be inferred using NDE techniques. Those could then be used in the integrated Paris Law relationship to output a prediction interval or distribution of estimated fatigue lives. This could aid designers and manufacturers by providing a clearer picture of estimated fatigue performance. Instead of a "one-point" estimate, a range could be provided giving a minimum and a maximum, ensuring performance requirements can be met through the part specifications.

## Contributions

Despite the limitations mentioned above, an effective specimen manufacturing, inspection, and testing process were developed to evaluate the influence of different cast indications on fatigue life. Additionally, this process was used to evaluate how varying cast surface textures may influence fatigue life in the presence of other indications. The impact of varying cast surface roughness on fatigue, as indicated in Chapter 1, has not been explored in the presence of other casting indications or in large parts before this research. Fatigue testing through the methods developed herein is to provide new means of evaluating factors that may influence casting performance. NDE techniques were investigated and tied to fatigue results where possible; indicating a need for further development of these processes and their potential to estimate cast part performance. This is through the final contribution of this research, which is the use of the Paris law and indication size to predict fatigue life, which can be used to develop NDE techniques. All of this contributes to casting designers' and founders' abilities to more efficiently produce cast parts that meet specific performance requirements and to develop the inspection techniques used to infer part performance.

## REFERENCES

[1] R. Shenoi and J. Xiong, Fatigue and Fracture Reliability Engineering, Springer-Verlag, 2011.

[2] "Constant Amplitude Stress-Life Technical Background," ALTAIR eFatigue, [Online]. Available: https://www.efatigue.com/constantamplitude/background/stresslife.html. [Accessed 16 October 2020].

[3] "S-N Fatigue Properties," NDT Resource Center, [Online]. Available: https://www.nde-ed.org/EducationResources/CommunityCollege/Materials/Mechanical/S-NFatigue.htm. [Accessed 25 April 2020].

[4] V. Radhakrishnan, "On Bilinearity of Manson-Coffin Low-Cycle-Fatigue Relationship," NASA, Madras, 1992.

[5] "Constant Amplitude Strain-Life Technical Background," ALTAIR eFatigue, [Online]. Available: https://www.efatigue.com/constantamplitude/background/strainlife.html. [Accessed 24 September 2020].

[6] G. Glinka, "The Fracture Mechanics Method," 2010. [Online]. Available: https://www.efatigue.com/training/Fracture_Mechanics_Method.pdf. [Accessed 6 9 2020].

[7] "Constant Amplitude Crack Growth Analysis," ALTAIR eFatigue, [Online]. Available: https://www.efatigue.com/constantamplitude/crackgrowth/#a. [Accessed 20 September 2020].

[8] E. Santecchia, A. M. S. Hamouda, F. Musharavati, E. Zalnezhad, M. Cabibbo, M. El Mehtedi and S. Spigarelli, "A Review on Fatigue Life Prediction Methods for Metals," *Advances in Materials Science and Engineering,* vol. 2016, 2016.

[9] M. Todinov, "A Probabilistic Method for Predicting Fatigue Life Controlled by Defects," *Materials Science and Engineering,* vol. 255, no. 1, pp. 117-123, 1998.

[10] A. Melander and M. Larsson, "The Effect of Stress Amplitude on the Cause of Fatigue Crack Initiation in a Spring Steel," *International Journal of Fatigue,* vol. 15, no. 2, pp. 119-131, 1993.

[11] A. de Bussac and J. C. Lautirdou, "A Probabilistic Model for Prediction of LCF Surface Crack Initiation in PM Alloys," *Fatigue & Fracture of Engineering Materials & Structures,* vol. 16, no. 8, pp. 861-874, 1993.

[12] A. de Bussac, "Prediction of the Competition Between Surface and Internal Fatigue Crack Initiation in PM Alloys," *Fatigue & Fracture of Engineering Materials & Structures,* vol. 17, no. 11, pp. 1319-1325, 1994.

[13] N. Horikawa, D. Sameshima, T. Nakamura and H. Oguma, "Effect of Casting Surface on Fatigue Properties of Thin-Wall Ductile Cast Iron," *Transactions of the Japan Society of Mechanical Engineers,* vol. 76, pp. 425-427, 2010.

[14] D. Roylance, "Introduction to Fracture Mechanics," Massachusetts Institute of Technology, Cambridge, 2001.

[15] S. K. Ås, B. Skallerud and B. W. Tveiten, "Surface Roughness Characterization for Fatigue Life Predictions Using Finite Element Analysis," *International Journal of Fatigue,* vol. 30, pp. 2200-2209, 2008.

[16] M. Blair, R. Monroe, C. Beckermann, R. Hardin, K. Carlson and C. Monroe, "Predicting the Occurrence and Effects of Defects in Castings," *JOM,* vol. 57, no. 5, pp. 29-34, 2005.

[17] C. Choi, W. R. Miller, D. A. Oberacker, G. K. Turnbull, J. F. Wallace and D. K. Wright, "Correlation of Destructive Testing of Steel Castings with Stress Analysis and Mechanical Properties," Steel Founders' Society of America, Cleveland, 1962.

[18] G. Daricilar and F. Peters, "Measurement Error of Visual Casting Surface Inspection," in *Steel Founders' Society of America - Technical and Operating Conference*, Chicago, 2005.

[19] R. Stone, K. Watts and F. Peters, "Visual Inspection: Known Factors that Affect Performance," in *Steel Founders' Society of America - Technical and Operating Conference*, Chicago, 2010.

[20] M. M. Voelker and F. Peters, "Development of a Digital Standard to Specify Surface Requirements of Cast Metal Surfaces," *ASTM Materials Performance and Characterization,* vol. 6, no. 2, 2017.

[21] M. M. Voelker, "Quantitative Surface Inspection Methods for Metal Castings," M.S. Thesis, Dept. of Industrial and Manufacturing Systems Engineering, Iowa State University, Ames, 2016.

[22] D. W. Shimpf and F. E. Peters, "Variogram Roughness Method for Casting Surface Characterization," *International Journal of Metalcasting,* 2020.

[23] "Introduction to Magnetic Particle Inpsection," NDT Resource Center, [Online]. Available: https://www.nde-ed.org/EducationResources/CommunityCollege/MagParticle/Introduction/introduction.htm. [Accessed 12 April 2020].

[24] R. Zheng and B. R. Ellingwood, "Role of Non-destructive Evaluation in Time-dependent Reliability Analysis," *Structural Safety,* vol. 20, pp. 325-339, 1998.

[25] M. Blair, R. Monroe, R. Hardin and C. Beckermann, "A New Standard for Radiographic Acceptance Criteria for Steel Castings," in *Proceedings of the 62nd SFSA Technical and Operating Conference*, Chicago, 2008.

[26] E. S. Breznak, C. Vishnevsky and J. F. Wallace, The Effect of Internal Shrinkage Discontinuities on the Fatigue and Impact Properties of Cast Steel Sections, Rocky River: Steel Founders' Society of America, 1969.

[27] K. M. Sigl, R. A. Hardin, R. I. Stephens and C. Beckermann, "Fatigue of 8630 Cast Steel in the Presence of Porosity," *International Journal of Cast Metals Research,* vol. 17, no. 3, pp. 130-146, 2004.

[28] A. Borbély, H. Mughrabi, G. Eisenmeier and H. Höppel, "A Finite Element Modelling Study of Strain Localization in the Vicinity of Near-surface Cavities as a Cause of Subsurface Fatigue Crack Initiation," *International Journal of Fracture,* vol. 115, pp. 227-232, 2002.

[29] J. Lai, H. Huang and W. Buising, "Effects of Microstructure and Surface Roughness on the Fatigue Strength of High-Strength Steels," *Procedia Strucural Integrity,* vol. 2, pp. 1213-1220, 2016.

[30] H. E. Boyer, Atlas of Fatigue Curves, Metals Park: American Society for Metals, 1986, pp. 1-10.

[31] G. Noll and C. Lipson, "Allowable Working Stresses," *Proceedings of the Society of Experimental Stress Analysis,* vol. 3, no. 2, pp. 89-101, 1946.

[32] E. Evans and L. Ebert, "Fatigue Properties of Comparable Cast and Wrought Steels," *Steel Founders' Society of America Research Report No. 35,* October 1955.

[33] R. Konečná, M. Kokavec and G. Nicoletto, "Surface Conditions and the Fatigue Behavior of Nodular Cast Iron," *Procedia Engineering,* vol. 10, pp. 2538-2543, 2011.

[34] J. A. Bannantine, J. J. Comer and J. L. Handrock, Fundamentals of Metal Fatigue Analysis, Englewood Cliffs: Prentice Hall, 1990.

[35] C. Vishnevsky, N. F. Bertolino and J. F. Wallace, "The Effects of Surface Discontinuities on the Fatigue Properties of Cast Steel Sections," Steel Foundry Research Foundation, Rocky River, 1966.

[36] Y. Murakami, "Stress Concentration," in *Metal Fatigue: Effects of Small Defects and Nonmetallic Inclusions*, Amsterdam, Academic Press, 2002, pp. 13-21.

[37] G. R. Irwin, "Analysis of Stresses and Strains Near the End of a Crack Traversing a Plate," *Journal of Applied Mechanics,* vol. 24, pp. 361-364, 1957.

[38] Y. Murakami and M. Endo, "Quantitative Evaluation of Fatigue Strength of Metals Containing Various Small Defects or Cracks," *Engineering Fracture Mechanics,* vol. 17, no. 1, pp. 1-15, 1983.

[39] S. McKelvey and A. Fatemi, "Surface Finish Effect on Fatigue Behavior of Forged Steel," *International Journal of Fatigue,* vol. 36, no. 1, pp. 130-145, 2012.

[40] P. Diekhoff, J. Hensel, T. Nitschke-Pagel and K. Dilger, "Investigation on Fatigue Strength of Cut Edges Produced by Various Cutting Methods for High-Strength Steels," *Welding in the World,* vol. 64, pp. 545-561, 2020.

[41] H. Itoga, K. Tokaji, M. Nakajima and H.-N. Ko, "Effect of Surface Roughness on Step-wise S-N Characteristics in High Strength Steel," *International Journal of Fatigue,* vol. 25, no. 5, pp. 379-385, 2003.

[42] ASTM E3024/E3024M-19, *Standard Practice for Magnetic Particle Testing for General Industry,* West Conshohocken: ASTM International, 2019.

[43] ASTM E466, *Standard Practice for Conducting Force Controlled Constant Amplitude Axial Fatigue Tests of Metallic Materials,* West Conshohocken: ASTM International, 2015.

[44] ASTM A802-19, *Standard Practice for Steel Castings, Surface Acceptance Standards, Visual Examination,* West Conshohocken: ASTM International, 2019.

[45] "Material Property Finder," ALTAIR eFatigue, [Online]. Available: https://www.efatigue.com/constantamplitude/crackgrowth/materials/. [Accessed 27 September 2020].